Mathematical analysis of an acoustically actuated nanospherical antenna with terahertz frequency range applications in the framework of generalized spectral magneto-electro-elastodynamic interface theory

Mohsen Farsiani [●],[1] Hossein M. Shodja [●],[1,2,*] and Ali Behzadan [●][3]

[1]*Department of Civil Engineering, Sharif University of Technology, P.O. Box 11155-9313, Tehran, Iran*
[2]*Center for Nanoscience and Nanotechnology, Institute for Convergence Science & Technology,*
Sharif University of Technology, Tehran 14588-89694, Iran
[3]*Department of Mathematics and Statistics, California State University Sacramento, Sacramento, California 95819, USA*

This paper undertakes a comprehensive exploration of multiphysics phenomena involving electromagnetic (EM) radiation emitted by a nanospherical piezoelectric scatterer embedded in a polymer matrix, subjected to P waves within the THz frequency spectrum. A nanosized piezoelectric scatterer as a potential antenna possesses a significant surface-to-volume ratio. Consequently, it becomes imperative to meticulously account for the nanoscopic polarization vector, residual polarization vector, stress field, and residual stress field at its interface with the surrounding matrix. The conventional electrodynamics theory falls short in addressing the problem of interest, primarily due to its oversight of the magneto-electro-elastic interface. One of the aims of the current work is to extend the previously devised mathematical framework of surface/interface elasticity theory for purely elastic medium at the nanoscale, to magneto-electro-elastic (MEE) medium. By harnessing the versatility of spherical harmonics, we have simultaneously solved the fully coupled elastodynamics and Maxwell's equations within the mathematical framework of spectral MEE surface/interface theory. In this study, we scrutinize specific nuances related to the introduced surface/interface characteristic lengths. This exploration enables us to examine the influence of size on EM radiated power, the fundamental resonance frequency, and the distribution of the magnetic field. The insights gained from our findings hold promise for the design of acoustically actuated nanospherical antennas, nanosensors, and nanoresonators utilizing piezoelectric nanospheres.

I. INTRODUCTION

Antennas play a critical and pervasive role in devices such as smartphones, tablets, radio frequency identification systems, and radars, converting alternating electric currents into electromagnetic (EM) wave radiation. Recent years have witnessed a surge in the applications of ultra-compact wireless communication systems [1], driving considerable efforts to downsize their components. Among these components, the antenna stands out as a crucial facilitator of EM wave transmission and reception. Consequently, there is a heightened demand for antennas that combine a compact size with high efficiency.

The forefront of antenna technology faces a significant challenge in the miniaturization of these devices [2–5]. Compact antennas, reliant on EM wave resonance, typically surpass one-tenth of the EM wavelength in size. This poses a formidable obstacle, particularly in achieving compact antennas and arrays, especially in the terahertz (THz) frequency ranges where wavelengths are substantial. The struggle for miniaturization imposes strict constraints on wireless communication systems. To overcome these challenges, it is imperative to explore novel antenna concepts. Focusing on innovative mechanisms for EM wave radiation and reception becomes crucial for the reduction of antenna size and the advancement of wireless communication systems.

Another important issue is that a primary goal of communication systems revolves around achieving the utmost data transmission speeds. Indeed, the ongoing escalation of data transfer rates in wireless communication systems, catering to both business and individual users, is prompting a substantial expansion of the bandwidths in use. Nevertheless, the ever-increasing user appetite for high-speed communication surpasses the capabilities of existing networks. Addressing this challenge entails exploring the integration of communication systems employing terahertz (THz) carrier frequencies [6].

Hence, considering the factors discussed earlier, there arises an immediate necessity to develop state-of-the-art ultracompact antennas capable of operating in the THz range.

Analytical and numerical inquiries into the interplay between acoustic waves and active materials have shed light on innovative pathways for designing compact antennas [7]. The phenomenon of EM emission from oscillating piezoelectric materials has a well-established history. In particular, AT-cut quartz plates have been the subject of several investigations; quartz crystals are cut to size based on precise

---

*shodja@sharif.edu

mathematical calculations, and even slight alterations can significantly impact the quality of the resulting part. Among the various angular cuts, the AT cut is widely employed. This specific cut is executed at an angle of 35 degrees from the z axis of the quartz crystal, making it one of the most commonly chosen cutting angles. Mindlin conducted an evaluation of EM radiation originating from an AT-cut quartz plate vibrating in the thickness shear mode [8]. Lee subsequently revisited Mindlin's investigation and explored EM radiation arising from a quartz sheet excited by an electric field [9]. Ballato reconsidered the latter problem by utilizing an equivalent circuit model [10]. The concept of piezoelectric antennas lay dormant until it reemerged in the early 2000s. During this period, the idea of utilizing vertically grown zinc oxide (ZnO) nanowire arrays to craft piezoelectric antennas gained much attention, as outlined in various fabrication-oriented papers [11–13].

In recent developments, magnetoelectric (ME) antennas, integrating the resonance of acoustic waves with the ME effect, have been showcased in the very-high frequency (VHF: 30-300 MHz) and ultra-high frequency (UHF: 0.3-3 GHz) bands. This represents a novel approach aimed at overcoming the constraints related to efficiency and dimensions encountered by conventional electrically small antennas [14–18]. In contrast to the conventional antennas that rely on oscillating charges to generate EM waves, ME antennas utilize the oscillation of magnetic dipole moments, which are activated by acoustic means at their electromechanical resonance frequency rather than the EM wave resonance frequency. Considering that acoustic waves propagate at significantly lower velocities compared to EM waves at the same operational frequency, this approach can result in a reduction of the size of antenna by one to two orders of magnitude (see, e.g., Ref. [18]).

As widely acknowledged, the size-independent traditional continuum theory proves inadequate in effectively modeling the physical and mechanical phenomena which are strongly influenced by the nanoscopic properties of the medium of interest. As a result, it is ill-suited for analyzing wave propagation with wavelengths comparable to the intrinsic length scales of the medium. These limitations stem from the intrinsic scale-free nature of classical continuum theories, rendering them incapable of addressing the discrete nature of matter and the associated surface/interface effects. Notably, atoms located in close proximity to a surface/interface exhibit substantial differences in the interatomic bond lengths and charge density distribution compared to those well within the bulk of the material. Consequently, understanding the electromechanical behavior of such nanostructures as nanosized piezoelectric antennas with a significant surface area-to-volume ratio demands specialized attention. For the treatment of problems involving purely elastic nanostructures, mathematical theory of surface/interface elasticity which is a size-dependent theory with high precision has been devised in Ref. [19]. In this theory which incorporates for the surface/interface effects exclusively within purely elastic materials, elastic solids are systematically divided into two interacting components: the bulk material and its complementary surface/interface domain.

The mathematical framework of surface/interface elasticity theory, as presented in [19,20] is concerned with the purely elastic media encapsulated by elastic surfaces/interfaces, and hence in its original context cannot be used to treat magneto-electro-elastic (MEE) media with bounding MEE surfaces/interfaces. Several researchers have employed an extended surface/interface model inspired by Gurtin and Murdoch [19] to explore piezoelectric effects [21–23]. Nevertheless, it is worth noting that all of these studies rely on the electroquasistatic approximation. A major drawback of the exclusion of Maxwell's equations is the limiting ability of their mathematical models to predict the electromagnetic wave propagation accurately. In order to circumvent this limitation, a recent study on the scattering of anti-plane shear waves by a piezoelectric nanofiber [24] has taken a different approach by treating its bounding interface as a separate piezoelectric domain in conjunction with the fully dynamic Maxwell's equations. However, the surface/interface piezoelectric theory in Ref. [24] is well-suited for the electro-quasistatic approximation and, moreover, their theory does not account for the surface/interface magnetization. Therefore the generalization of interface elasticity [19,20] to tackle fully dynamic problems involving nanosized piezoelectric antenna with MEE interface becomes indispensable, as such is one of the aims of the present work. In the literature, the electric current has been considered through the interface of a bimaterial, regardless of the size [25]. The concepts like surface electric polarization as discussed in Ref. [26], and magnetization, as detailed in Refs. [27,28] are instrumental in the development of the current theory. In the present work, we are dealing with a nanosized piezoelectric particle embedded in a polymer matrix. As we shall see, the alteration of the applied time-dependent strain field, due to the time-harmonic incident P waves, results in moving polarization, inducing effective magnetization density.

Scalar, vector, and tensor spherical harmonics are fundamental components in diverse areas of mathematical physics. Notably, they play a critical role in quantum mechanics, serving as a key tool for characterizing the angular momentum of particles (as discussed in, for example, Ref. [29]). Additionally, the utilization of spherical harmonics to expand field quantities has proven to be a highly effective strategy for addressing challenges in micromechanics of inhomogeneities [30,31]. Moreover, these versatile tools exhibit significant potential in tackling piezoelectric problems characterized by spherical geometry and a wide range of electromechanical loadings, as discussed in Ref. [32]. For a more comprehensive exploration of spherical harmonics from a mathematical perspective, readers can refer to Ref. [33].

In this work, we extend the surface/interface elasticity theory, originally developed for purely elastic media, to encompass electrodynamics in MEE media. Subsequently, given the spherical geometry of the piezoelectric particle, the formulations are presented in spherical coordinates. Furthermore, for a rigorous mathematical analysis, we employ the aforementioned spherical harmonics to study the behavior of the acoustically actuated nanospherical piezoelectric particle embedded in a polymer matrix subjected to THz frequency range.

This paper is structured as follows. Section II provides a description of the problem statement and the model. Section III is dedicated to the generalization of the Gurtin-Murdoch theory to MEE surfaces/interfaces. In Sec. IV an
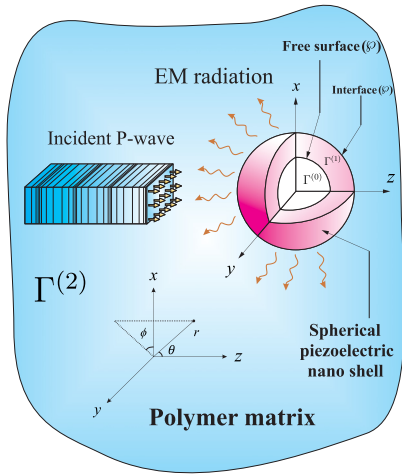
FIG. 1. The nomenclature of a proposed media.

introduction of the spectral theory of the MEE fields and their governing equations is presented. The derivation of the spectral MEE equations is detailed in Sec. V, while Sec. VI focuses on presenting the spectral surface/interface boundary conditions. Section VII provides the solution to the governing spectral boundary value problem (BVP). In Sec. VIII, the calculation of electromagnetic radiated power is discussed. Section IX delves into several examples showcasing the diverse applications of the proposed method. Finally, the paper concludes in Sec. X.

II. STATEMENT OF THE PROBLEM

Consider an isotropic homogeneous polymer matrix, denoted by $\Gamma^{(2)}$, surrounding a nanospherical piezoelectric shell with inner radius R_1 and outer radius R_2, which we denote by $\Gamma^{(1)}$, as shown in Fig. 1. A complete description of the regions depicted in Fig. 1 is as follows:

$$
\begin{aligned}
r < R_1 & \quad \text{nanovoid } (\Gamma^{(0)}) \\
r = R_1 & \quad \text{free surface } (\wp) \\
R_1 < r < R_2 & \quad \text{piezoelectric shell } (\Gamma^{(1)}) \\
r = R_2 & \quad \text{interface } (\wp) \\
r > R_2 & \quad \text{polymer matrix } (\Gamma^{(2)}).
\end{aligned}
\tag{1}
$$

The superscript $\wp$ over a field quantity implies that the quantity is associated with the interface or the free surface. Moreover, the superscripts "(0)," "(1)," and "(2)" indicate that the given quantity belongs to the nanovoid, shell, and matrix, respectively. The origin of the Cartesian coordinate system (x, y, z) and the spherical coordinate system (r, θ, ϕ) coincide with the center of the spherical shell as depicted in Fig. 1. Furthermore, for conciseness, we let $(\Omega) \equiv (\theta, \phi)$. We assume perfect bonding and coherent shell-matrix interface. The nano piezoelectric shell is assumed to be spherically isotropic and at each point the polling direction is radially oriented. The system is stimulated by a high-frequency mechanical time harmonic P wave with angular frequency ω propagating in

the positive z-direction. Considering that the problem of interest is concerned with an embedded nanosize spherical shell, the frequency of the incident P-wave applicable to such a system must be in THz range. In this work, we will derive and solve the governing system of differential equations with the appropriate boundary conditions, describing the fully coupled magneto-electro-elastic (MEE) fields for this problem. In particular, we will pay careful attention to the effects of the interface on the determination of field quantities.

Our approach for solving the governing system of partial differential equations will be based on the expansion method in terms of spherical harmonics and can be viewed as an extension of the spectral analysis framework developed by Khorshidi and Shodja in Ref. [34]. The spectral theory framework in Ref. [34] was shown to be particularly helpful in treating problems with spherical geometries. Here, in our augmented framework we will be able to address the case of nanosize spherically isotropic piezoelectric media.

Suppose there are no body forces, electric charges, and current densities in both the matrix and the shell. The elastodynamics equation of motion and the Maxwell's equations governing the proposed problem are

$$
\operatorname{div}_{\mathbb{R}^3} \bar{\boldsymbol{\sigma}} = \rho \frac{\partial^2 \bar{\mathbf{u}}}{\partial^2 t}, \tag{2}
$$

$$
\operatorname{curl}_{\mathbb{R}^3} \bar{\mathbf{E}} = -\frac{\partial \bar{\mathbf{B}}}{\partial t}, \tag{3a}
$$

$$
\operatorname{curl}_{\mathbb{R}^3} \bar{\mathbf{H}} = \frac{\partial \bar{\mathbf{D}}}{\partial t}, \tag{3b}
$$

$$
\operatorname{div}_{\mathbb{R}^3} \bar{\mathbf{D}} = 0, \tag{3c}
$$

$$
\operatorname{div}_{\mathbb{R}^3} \bar{\mathbf{B}} = 0, \tag{3d}
$$

where $\rho, \bar{\boldsymbol{\sigma}}, \bar{\mathbf{u}}, \bar{\mathbf{E}}, \bar{\mathbf{H}}, \bar{\mathbf{D}}$, and $\bar{\mathbf{B}}$ indicate, respectively, the mass density, stress field, displacement field, electric field, magnetic field, electric displacement, and magnetic flux density. Here we look for solutions where the time variation of all the MEE field variables $(\bar{\boldsymbol{\sigma}}, \bar{\mathbf{u}}, \bar{\mathbf{E}}, \bar{\mathbf{H}}, \bar{\mathbf{D}})$ is assumed to be harmonic with angular velocity ω according to $\bar{\psi}(r, \Omega, t) = \psi(r, \Omega)e^{-\iota\omega t}$ in which $\iota = \sqrt{-1}$. That is, we are seeking solutions of the following form:

$$
\bar{\mathbf{u}}(r, \Omega, t) = \mathbf{u}(r, \Omega)e^{-\iota\omega t},
$$

$$
\bar{\boldsymbol{\sigma}}(r, \Omega, t) = \boldsymbol{\sigma}(r, \Omega)e^{-\iota\omega t},
$$

$$
\bar{\mathbf{E}}(r, \Omega, t) = \mathbf{E}(r, \Omega)e^{-\iota\omega t},
$$

$$
\bar{\mathbf{H}}(r, \Omega, t) = \mathbf{H}(r, \Omega)e^{-\iota\omega t},
$$

$$
\bar{\mathbf{D}}(r, \Omega, t) = \mathbf{D}(r, \Omega)e^{-\iota\omega t},
$$

$$
\bar{\mathbf{B}}(r, \Omega, t) = \mathbf{B}(r, \Omega)e^{-\iota\omega t}. \tag{4}
$$

Such solutions will be referred to as the time harmonic solutions. As we shall see, it will be demonstrated that there exists a solution to our boundary value problem (BVP) where all the MEE fields are time harmonic and so our aforementioned assumption on the form of the field variables is consistent with the interrelationships between variables that appear in the equations. Using Eq. (4), we may rewrite Eqs. (2) and

(3a)–(3d) as follows:

$$\text{div}_{\mathbb{R}^3}\boldsymbol{\sigma} + \rho\omega^2\mathbf{u} = 0, \tag{5}$$

$$\text{curl}_{\mathbb{R}^3}\mathbf{E} = \iota\omega\mathbf{B}, \tag{6a}$$

$$\text{curl}_{\mathbb{R}^3}\mathbf{H} = -\iota\omega\mathbf{D}, \tag{6b}$$

$$\text{div}_{\mathbb{R}^3}\mathbf{D} = 0, \tag{6c}$$

$$\text{div}_{\mathbb{R}^3}\mathbf{B} = 0. \tag{6d}$$

It should be noted that Eqs. (6c) and (6d) can be obtained by taking the divergence of Eqs. (6b) and (6a), respectively.

Assuming that the deformations are small, the strain tensor $\boldsymbol{\epsilon}$ can be expressed in term of the gradient of the elastic displacement field $\mathbf{u}$ as

$$\boldsymbol{\epsilon} = \tfrac{1}{2}(\nabla_{\mathbb{R}^3}\mathbf{u} + (\nabla_{\mathbb{R}^3}\mathbf{u})^T). \tag{7}$$

In general,

$$\begin{aligned} \boldsymbol{\sigma} &= \mathbf{C} : \boldsymbol{\epsilon} - (\mathbf{e})^T \cdot \mathbf{E}, \\ \mathbf{D} &= \kappa_0\mathbf{E} + \mathbf{P} = \mathbf{e} : \boldsymbol{\epsilon} + \boldsymbol{\kappa} \cdot \mathbf{E}, \\ \mathbf{B} &= \mu_0(\mathbf{H} + \mathbf{M}). \end{aligned} \tag{8}$$

Here, $\mathbf{C}$, $\mathbf{e}$, and $\boldsymbol{\kappa}$ are the elastic moduli tensor and the piezoelectric tensor, and the dielectric tensor, respectively. κ_0, μ_0, $\mathbf{P}$, and $\mathbf{M}$ are vacuum permittivity, vacuum magnetic permeability, electric polarization, and magnetization, respectively. Hereafter, when any of the superscripts "$\Re$," "I," or "$\Im$" appears over a field quantity, it indicates that the quantity corresponds to the refracted field, incident field, or scattered field, respectively. Note that for the problem under consideration the MEE fields can written as

$$\mathbf{u} = \begin{cases} \mathbf{u}^{\Re(1)}, & R_1 < r < R_2 \\ \mathbf{u}^{I(2)} + \mathbf{u}^{\Im(2)}, & r > R_2 \end{cases}, \tag{9a}$$

$$\mathbf{E} = \begin{cases} \mathbf{E}^{\Re(0)}, & r < R_1 \\ \mathbf{E}^{\Re(1)}, & R_1 < r < R_2, \\ \mathbf{E}^{\Im(2)}, & r > R_2 \end{cases} \tag{9b}$$

$$\mathbf{H} = \begin{cases} \mathbf{H}^{\Re(0)}, & r < R_1 \\ \mathbf{H}^{\Re(1)}, & R_1 < r < R_2. \\ \mathbf{H}^{\Im(2)}, & r > R_2 \end{cases} \tag{9c}$$

In the present work, we assume the displacement field due to the incident P-wave is given by

$$u_x^{I(2)}(x, y, z, t) = 0, \tag{10a}$$

$$u_y^{I(2)}(x, y, z, t) = 0, \tag{10b}$$

$$u_z^{I(2)}(x, y, z, t) = \Lambda e^{\iota(K_p z - \omega t)}, \tag{10c}$$

that is, we assume that the P wave is a harmonic plane wave with angular velocity ω and amplitude Λ in the z direction. Here, K_p is the compressive wave number given by

$$K_p = \frac{\omega}{C_p}, \tag{11}$$

where $C_p = \sqrt{\frac{\lambda + 2\mu}{\rho}}$ is the velocity of the compressive wave, and λ and μ are Lame' constants of the polymer matrix. As we shall see, the constitutive equations of the spherically isotropic

piezoelectric region can be represented more conveniently using spherical coordinates (r, θ, ϕ). Indeed, let us denote the standard orthonormal basis associated with the spherical coordinates (r, θ, ϕ), by $\mathbf{e}_r$, $\mathbf{e}_\theta$, $\mathbf{e}_\phi$. Then the MEE fields can be expanded as follows:

$$\begin{aligned} \mathbf{u} &= u_i\mathbf{e}_i, \\ \boldsymbol{\epsilon} &= \epsilon_{ij}\mathbf{e}_i \otimes \mathbf{e}_j, \qquad \text{in } \Gamma^{(1)} \cup \Gamma^{(2)}; \\ \boldsymbol{\sigma} &= \sigma_{ij}\mathbf{e}_i \otimes \mathbf{e}_j, \end{aligned} \tag{12}$$

$$\begin{aligned} \mathbf{E} &= E_i\mathbf{e}_i, \\ \mathbf{D} &= D_i\mathbf{e}_i, \\ \mathbf{H} &= H_i\mathbf{e}_i, \qquad \text{in } \Gamma^{(0)} \cup \Gamma^{(1)} \cup \Gamma^{(2)}. \\ \mathbf{B} &= B_i\mathbf{e}_i. \end{aligned} \tag{13}$$

Here, $i, j = r, \theta, \phi$. In order to write the constitutive relations, we will make use of the following notation for the components of the elastic moduli tensor $\mathbf{C}$, the piezoelectric tensor $\mathbf{e}$, and the dielectric tensor $\boldsymbol{\kappa}$:

$$\begin{aligned} & C_{11} = C_{22} = C_{\theta\theta\theta\theta} = C_{\phi\phi\phi\phi}, \quad C_{12} = C_{\theta\theta\phi\phi}, \\ & C_{13} = C_{23} = C_{\theta\theta rr} = C_{\phi\phi rr}, \quad C_{33} = C_{rrrr}, \\ & C_{44} = C_{r\phi r\phi} = C_{r\theta r\theta}, \quad e_{31} = e_{32} = e_{r\theta\theta} = e_{r\phi\phi}, \\ & e_{33} = e_{rrr}, \quad e_{15} = e_{\phi\phi r} = e_{\theta\theta r}, \\ & \kappa_{11} = \kappa_{22} = \kappa_{\theta\theta} = \kappa_{\phi\phi}, \quad \kappa_{33} = \kappa_{rr}, \\ & \mu_{11} = \mu_{22} = \mu_{\theta\theta} = \mu_{\phi\phi}, \quad \mu_{33} = \mu_{rr}. \end{aligned} \tag{14}$$

Subsequently, the constitutive relations (8) for the spherically isotropic piezoelectric shell can be conveniently expressed as follows (see, e.g., Ref. [35]):

$$\begin{aligned} \sigma_{\theta\theta} &= C_{11}\epsilon_{\theta\theta} + C_{12}\epsilon_{\phi\phi} + C_{13}\epsilon_{rr} - e_{31}E_r, \\ \sigma_{\phi\phi} &= C_{12}\epsilon_{\theta\theta} + C_{11}\epsilon_{\phi\phi} + C_{13}\epsilon_{rr} - e_{31}E_r, \\ \sigma_{rr} &= C_{13}\epsilon_{\theta\theta} + C_{13}\epsilon_{\phi\phi} + C_{33}\epsilon_{rr} - e_{33}E_r, \\ \sigma_{r\theta} &= 2C_{44}\epsilon_{r\theta} - e_{15}E_\theta, \\ \sigma_{r\phi} &= 2C_{44}\epsilon_{r\phi} - e_{15}E_\phi, \\ \sigma_{\theta\phi} &= (C_{11} - C_{12})\epsilon_{\theta\phi}, \quad \text{in } \Gamma^{(1)} \\ D_\theta &= 2e_{15}\epsilon_{r\theta} + k_{11}E_\theta, \\ D_\phi &= 2e_{15}\epsilon_{r\phi} + k_{11}E_\phi, \\ D_r &= e_{31}\epsilon_{\theta\theta} + e_{31}\epsilon_{\phi\phi} + e_{33}\epsilon_{rr} + k_{33}E_r, \\ B_\theta &= \mu_{11}H_\theta, \\ B_\phi &= \mu_{11}H_\phi, \\ B_r &= \mu_{33}H_r. \end{aligned} \tag{15}$$

Moreover, the constitutive relations for the elastic polymer matrix may be written as

$$\begin{aligned} \sigma_{ij} &= 2\mu\epsilon_{ij} + \lambda tr(\boldsymbol{\epsilon})\delta_{ij}, \\ D_i &= \kappa_m E_i, \qquad \text{in } \Gamma^{(2)}. \\ B_i &= \mu_m H_i, \end{aligned} \tag{16}$$

Here, $i, j = r, \theta, \phi$, and λ and μ are Lame' constants, κ_m is the dielectric constant of the matrix, and μ_m is the magnetic permeability for the matrix.
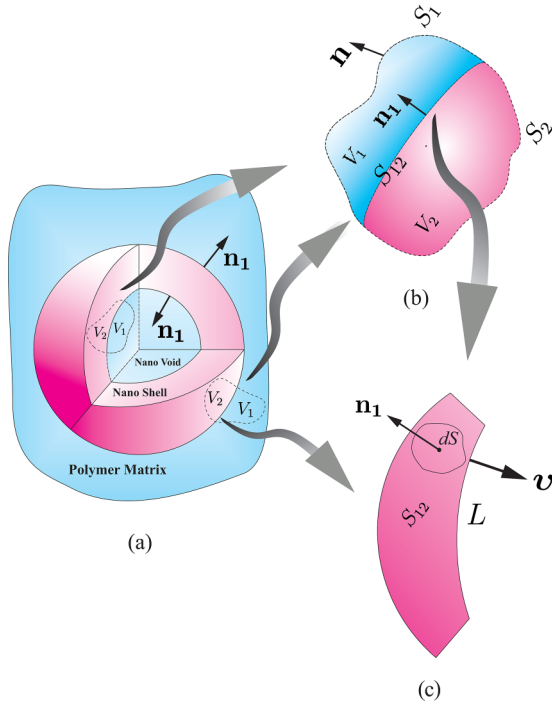
FIG. 2. Two adjacent MEE regions V_1 and V_2 with boundary surfaces S_1 and S_2.

III. GENERALIZATION OF THE GURTIN-MURDOCH THEORY TO MEE SURFACES/INTERFACES

Since the embedded piezoelectric shell considered herein is nanosize, the effects of its MEE interface with the polymer matrix and its MEE free inner surface are nonnegligible. To this end, the mathematical framework of surface elasticity developed by Gurtin and Murdoch in Ref. [19] for purely elastic surfaces/interfaces is generalized to MEE surfaces/interfaces in the present work. In particular, in what follows, we will develop a surface/interface theory in which the electromagnetic effects of the interface are taken into account.

Consider two adjacent MEE regions V_1 and V_2 with boundary surfaces S_1 and S_2 bonded across an surface/interface S_{12} as shown in Fig. 2. For example, think of S_{12} as a portion of interface, V_1 as a portion of the polymer matrix, and V_2 as a portion of the piezoelectric shell (or think of S_{12} as a portion of free surface, V_1 as a portion of the nanovoid, and V_2 as a portion of the piezoelectric shell). Let L denote the boundary of S_{12} and $\boldsymbol{v}$ be the outward unit normal vector to L.

According to Gurtin-Murdoch surface elasticity theory, assuming that the displacement field **u** on the surface has the form $\bar{\mathbf{u}}^{\wp} = \mathbf{u}^{\wp}e^{-\iota\omega t}$, the corresponding elastodynamic equations of motion of an surface/interface with unit outward normal vector **n** is given by

$$\text{div}_{\wp}\boldsymbol{\sigma}^{\wp} + [\boldsymbol{\sigma}.\mathbf{n}] = -\rho^{\wp}\omega^2\mathbf{u}^{\wp}, \qquad (17)$$

where $\boldsymbol{\sigma}^{\wp}$ is the interface stress tensor, $\rho^{\wp}$ denotes the interface mass density, and $[\boldsymbol{\sigma}.\mathbf{n}] = (\boldsymbol{\sigma}.\mathbf{n})_{\text{out}} - (\boldsymbol{\sigma}.\mathbf{n})_{\text{in}}$ denotes the jump in the quantity $\boldsymbol{\sigma}.\mathbf{n}$ across the surface/interface, and $\text{div}_{\wp}$ denotes the surface divergence (see Appendix D). The surface/interface equation of motion (17) was originally given in Ref. [20] for purely elastic media in the absence of

electromagnetic effects. Now, by using Eqs. (6a), and (8) for V_1 and V_2, respectively, we have

$$\iiint_{V_1}(\text{curl}_{\mathbb{R}^3}\mathbf{E}_1)dV = \iiint_{V_1}\iota\omega\mu_0(\mathbf{H}_1 + \mathbf{M}_1)dV, \quad (18a)$$

$$\iiint_{V_2}(\text{curl}_{\mathbb{R}^3}\mathbf{E}_2)dV = \iiint_{V_2}\iota\omega\mu_0(\mathbf{H}_2 + \mathbf{M}_2)dV. \quad (18b)$$

In the above equations, the subscripts "1" and "2" indicate that the given quantity belongs to V_1 and V_2, respectively. If we apply the Stokes' theorem to Eqs. (18a) and (18b), we will obtain

$$\iint_{S_1}(\mathbf{n} \times \mathbf{E}_1)dS - \iint_{S_{12}}(\mathbf{n}_1 \times \mathbf{E}_1)dS$$
$$= \iiint_{V_1}\iota\omega\mu_0(\mathbf{H}_1 + \mathbf{M}_1)dV, \qquad (19a)$$

$$\iint_{S_2}(\mathbf{n} \times \mathbf{E}_2)dS + \iint_{S_{12}}(\mathbf{n}_1 \times \mathbf{E}_2)dS$$
$$= \iiint_{V_2}\iota\omega\mu_0(\mathbf{H}_2 + \mathbf{M}_2)dV. \qquad (19b)$$

Let $V = V_1 \cup V_2$ and $S = S_1 \cup S_2$. In the presence of surface/interface magnetization $\mathbf{M}^{\wp}$ ([27,28]), we have $\mathbf{B} = \mu_0(\mathbf{H} + \mathbf{M})$ where analogous to Ref. [25] we may write

$$\iiint_V\mathbf{M}dV = \iiint_{V_1}\mathbf{M}_1dV + \iiint_{V_2}\mathbf{M}_2dV + \iint_{S_{12}}\mathbf{M}^{\wp}dS,$$

$$\iiint_V\mathbf{H}dV = \iiint_{V_1}\mathbf{H}_1dV + \iiint_{V_2}\mathbf{H}_2dV. \qquad (20)$$

It follows from Eqs. (19a), (19b), and (20) that

$$\iint_S(\mathbf{n} \times \mathbf{E})dS - \iint_{S_{12}}\mathbf{n}_1 \times (\mathbf{E}_1 - \mathbf{E}_2)dS$$
$$= \iiint_V\iota\omega\mathbf{B}dV - \iint_{S_{12}}\iota\omega\mu_0\mathbf{M}^{\wp}dS. \qquad (21)$$

Similarly, it follows from Eqs. (8) and (6b), the Stokes' theorem, and the following relation for the total electric polarization in the presence of surface/interface polarization $\mathbf{P}^{\wp}$ ([26]):

$$\iiint_V\mathbf{P}dV = \iiint_{V_1}\mathbf{P}_1dV + \iiint_{V_2}\mathbf{P}_2dV + \iint_{S_{12}}\mathbf{P}^{\wp}dS, \qquad (22)$$

that

$$\iint_S(\mathbf{n} \times \mathbf{H})dS - \iint_{S_{12}}\mathbf{n}_1 \times (\mathbf{H}_1 - \mathbf{H}_2)dS$$
$$= \iiint_V -\iota\omega\mathbf{D}dV + \iint_{S_{12}}\iota\omega\mathbf{P}^{\wp}dS. \qquad (23)$$

Under the assumption that the field quantities are continuous everywhere in V, the integral forms of Faraday's law and Ampere's law are expressed as ([36]) $\iint_S(\mathbf{n} \times \mathbf{E})dS = \iiint_V\iota\omega\mathbf{B}dV$ and $\iint_S(\mathbf{n} \times \mathbf{H})dS = \iiint_V -\iota\omega\mathbf{D}dV$. Now, in the presence of the electric and magnetic field discontinuities across surface/interface, if we postulate the subsequent

boundary conditions at the surface/interface S_{12} [25]:

$$\mathbf{n}_1 \times [\mathbf{E}] - \iota\omega\mu_0\mathbf{M}^{\wp} = 0, \tag{24a}$$

$$\mathbf{n}_1 \times [\mathbf{H}] + \iota\omega\mathbf{P}^{\wp} = 0, \tag{24b}$$

then these conditions will guarantee that $\iint_S (\mathbf{n} \times \mathbf{E})dS = \iiint_V \iota\omega\mathbf{B}dV$, and $\iint_S (\mathbf{n} \times \mathbf{H})dS = \iiint_V -\iota\omega\mathbf{D}dV$, maintaining the same form as in the continuous case, but now, due to our postulates, we see that they are still applicable even when the fields exhibit discontinuities across the surface/interface. From a physical standpoint, it is noteworthy from (24a) and (24b) that an effective magnetic polarization current can be induced in a surface/interface without magnetic polarizability, and similarly, an electric polarization current can be generated in a surface/interface without electric polarizability. We note that, alternatively, one could express equivalently the boundary conditions (24a) and (24b) on the surface/interface in terms of **B** and **D** (instead of **E** and **H**). Following Ref. [24], we make the assumption that the tangential component of the electric field is continuous across the surface/interface S_{12}, that is $\mathbf{n}_1 \times [\mathbf{E}] = 0$. Considering Eq. (24a), this assumption immediately tells us that the interface magnetization $\mathbf{M}^{\wp}$ vanishes on S_{12}. Of course, note that the magnetization in the bulk is not necessarily zero.

At this point, let us summarize the governing equations for our free surface/interface. Assuming coherent MEE interface, we have

$$[\mathbf{u}] = 0, \quad \text{on } r = R_2, \tag{25a}$$

$$[\boldsymbol{\sigma}.\mathbf{n}] + \text{div}_{\wp}\boldsymbol{\sigma}^{\wp} = -\rho^{\wp}\omega^2\mathbf{u}^{\wp}, \quad \text{on } r = R_1, \text{ and } r = R_2, \tag{25b}$$

$$\mathbf{n} \times [\mathbf{E}] = 0, \quad \text{on } r = R_1, \text{ and } r = R_2, \tag{25c}$$

$$\mathbf{n} \times [\mathbf{H}] + \iota\omega\mathbf{P}^{\wp} = 0, \quad \text{on } r = R_1, \text{ and } r = R_2. \tag{25d}$$

These equations serve as boundary conditions with which the governing equations of the medium (5), (6a), and (6b) are equipped.

Now, we will describe the strain-displacement relations for our spherical surface/interface. First note that the displacement field on the surface/interface can be expressed as

$$\mathbf{u}^{\wp}(\Omega) = u_r^{\wp}(\Omega)\mathbf{e}_r + u_\theta^{\wp}(\Omega)\mathbf{e}_\theta + u_\phi^{\wp}(\Omega)\mathbf{e}_\phi. \tag{26}$$

According to [19], the surface/interface strain field is given by

$$\boldsymbol{\epsilon}^{\wp} = \tfrac{1}{2}((\mathcal{D}\mathbf{u}^{\wp t}) + (\mathcal{D}\mathbf{u}^{\wp t})^T) - u^{\wp n}\mathbf{L}, \tag{27}$$

in which $\mathbf{u}^{\wp t}$ is the displacement vector tangent to the surface, $u^{\wp n}$ is the normal component of surface displacement, and **L** is the Weingarten map of the surface (see Appendix E for details). Here $\mathcal{D}\mathbf{u}^{\wp t}$ is the tangential part of $\nabla_{\wp}\mathbf{u}^{\wp t}$ where $\nabla_{\wp}$ is the surface gradient (see Appendix D for details). It follows from Eq. (27) and formula (D2) that the components of the surface/interface strain field can be written as follows:

$$\epsilon_{rr}^{\wp}(\Omega) = \epsilon_{r\theta}^{\wp}(\Omega) = \epsilon_{r\phi}^{\wp}(\Omega) = 0, \tag{28a}$$

$$\epsilon_{\theta\theta}^{\wp}(\Omega) = \frac{1}{R}\left(u_r^{\wp}(\theta, \phi) + \frac{\partial u_\theta^{\wp}(\theta, \phi)}{\partial\theta}\right), \tag{28b}$$

$$\epsilon_{\theta\phi}^{\wp}(\Omega) = \frac{1}{2R}\left(\frac{1}{\sin\theta}\left(\frac{\partial u_\theta^{\wp}(\theta, \phi)}{\partial\phi} - u_\phi^{\wp}(\theta, \phi)\cos\theta\right) + \frac{\partial u_\phi^{\wp}(\theta, \phi)}{\partial\theta}\right), \tag{28c}$$

$$\epsilon_{\phi\phi}^{\wp}(\Omega) = \frac{1}{R}\left(\frac{1}{\sin\theta}\left(\frac{\partial u_\phi^{\wp}(\theta, \phi)}{\partial\phi} + u_\theta^{\wp}(\theta, \phi)\cos\theta\right) \tag{28d}$$

$$+ u_r^{\wp}(\theta, \phi)\right). \tag{28e}$$

Here, $R = R_1$ if $\wp$ represents the free surface and $R = R_2$ if $\wp$ represents the interface.

Finally, we utilize the work of Ref. [37] to write the general constitutive equations of piezoelectric surface/interface as follows:

$$\boldsymbol{\sigma}^{\wp} = \boldsymbol{\sigma}_0 + \mathbf{C}^{\wp} : \boldsymbol{\epsilon}^{\wp} - (\mathbf{e}^{\wp})^T \cdot \mathbf{E}^{\wp}, \tag{29}$$

$$\mathbf{P}^{\wp} = \mathbf{P}_0 + \mathbf{e}^{\wp} : \boldsymbol{\epsilon}^{\wp} + \boldsymbol{\gamma}^{\wp} \cdot \mathbf{E}^{\wp}, \tag{30}$$

where $\boldsymbol{\sigma}_0$ is the residual surface/interface stress tensor and $\mathbf{P}_0$ is the residual surface/interface electric polarization vector. $\mathbf{C}^{\wp}$, $\mathbf{e}^{\wp}$, and $\boldsymbol{\gamma}^{\wp}$ are surface elastic tensor, surface piezoelectric tensor, and surface electric polarizability tensor, respectively. Since the medium under consideration is spherically isotropic, meaning that the constitutive behavior is invariant under rotation, and considering the implications of this rotational symmetry which can be viewed in Eq. (15), we can obtain the following constitutive relations for the surface/interface:

$$\sigma_{\theta\theta}^{\wp} = (\boldsymbol{\sigma}_0)_{\theta\theta} + C_{11}^{\wp}\epsilon_{\theta\theta}^{\wp} + C_{12}^{\wp}\varepsilon_{\phi\phi}^{\wp}, \tag{31a}$$

$$\sigma_{\phi\phi}^{\wp} = (\boldsymbol{\sigma}_0)_{\phi\phi} + C_{12}^{\wp}\varepsilon_{\theta\theta}^{\wp} + C_{11}^{\wp}\varepsilon_{\phi\phi}^{\wp}, \tag{31b}$$

$$\sigma_{\theta\phi}^{\wp} = (\boldsymbol{\sigma}_0)_{\theta\phi} + (C_{11}^{\wp} - C_{12}^{\wp})\varepsilon_{\theta\phi}^{\wp}, \tag{31c}$$

$$P_\theta^{\wp} = (\mathbf{P}_0)_\theta + \gamma_{11}^{\wp}E_\theta, \tag{31d}$$

$$P_\phi^{\wp} = (\mathbf{P}_0)_\phi + \gamma_{11}^{\wp}E_\phi. \tag{31e}$$

Here,

$$C_{11}^{\wp} = \hat{m}_1 C_{11}, \tag{32}$$

$$C_{12}^{\wp} = \hat{m}_2 C_{12}, \tag{33}$$

$$\gamma_{11}^{\wp} = \hat{m}_3 \kappa_{11}, \tag{34}$$

in which $\hat{m}_i'$s, $1 \leqslant i \leqslant 3$ are characteristic lengths of the surface/interface. Also, we let $\hat{m}_4 = \frac{\rho}{\rho^{\wp}}$. Within Gurtin-Murdoch surface elasticity theory, the nonzero surface traction (force per unit length) along any arbitrary cut on the surface is tangent to the surface and the surface stress components $\sigma_{rr}^{\wp}, \sigma_{r\theta}^{\wp}, \sigma_{r\phi}^{\wp}$ are zero. Likewise, the radial component of the surface polarization, $P_r^{\wp}$ is zero.

$$\sigma_{rr}^{\wp} = \sigma_{r\theta}^{\wp} = \sigma_{r\phi}^{\wp} = P_r^{\wp} = 0. \tag{35}$$

IV. SPECTRAL ANALYSIS OF THE MEE FIELDS AND THEIR GOVERNING EQUATION

Our main strategy in analyzing the problem under consideration is to transform the governing BVP [Eqs. (5), (6a), (6b), and (25a)–(25d)] which involves tensor PDEs into a system

of ordinary differential equations (ODEs). As we shall see, this goal can be achieved by expanding the unknown fields appearing in the equations in terms of the spherical harmonics. A detailed discussion on spherical harmonics can be found in Appendix A. Indeed, the unknown MEE fields in our problem can be expanded in terms of spherical harmonics as follows:

$$\mathbf{u}(r;\Omega) = \sum_{l,m} \sum_{i=1}^{3} u_i^{l,m}(r) \mathbf{V}_i^{l,m}(\Omega), \tag{36}$$

$$\{\mathbf{D}(r;\Omega), \mathbf{E}(r;\Omega)\}$$

$$= \sum_{l,m} \sum_{i=1}^{3} \{D_i^{l,m}(r), E_i^{l,m}(r)\} \mathbf{V}_i^{l,m}(\Omega), \tag{37}$$

$$\{\mathbf{B}(r;\Omega), \mathbf{H}(r;\Omega)\}$$

$$= \sum_{l,m} \sum_{i=1}^{3} \{B_i^{l,m}(r), H_i^{l,m}(r)\} \mathbf{V}_i^{l,m}(\Omega), \tag{38}$$

$$\{\boldsymbol{\epsilon}(r;\Omega), \boldsymbol{\sigma}(r;\Omega)\}$$

$$= \sum_{l,m} \sum_{i=1}^{6} \{\epsilon_i^{l,m}(r), \sigma_i^{l,m}(r)\} \mathbf{T}_i^{l,m}(\Omega), \tag{39}$$

$$\{\mathbf{u}^{\wp}(\Omega), \mathbf{P}^{\wp}(\Omega)\}$$

$$= \sum_{l,m} \sum_{i=1}^{3} \{u_i^{l,m;\wp}, P_i^{l,m;\wp}\} \mathbf{V}_i^{l,m}(\Omega), \tag{40}$$

$$\{\boldsymbol{\epsilon}^{\wp}(\Omega), \boldsymbol{\sigma}^{\wp}(\Omega)\}$$

$$= \sum_{l,m;\wp} \sum_{i=1}^{6} \{\epsilon_i^{l,m;\wp}, \sigma_i^{l,m;\wp}\} \mathbf{T}_i^{l,m}(\Omega). \tag{41}$$

Here we will use the above expansions to transform equations Eqs. (5), (6a), and (6b) into a system of ODEs with certain boundary conditions obtained from Eqs. (25a)–(25d). It is important to note that due to the rotational symmetry of the problem, the mechanical and electromagnetic fields are independent of ϕ, hence only the modes with $m = 0$ have nonzero coefficients in the above expansions; for $m = 0$, $P_{l,0}$ is the Legendre polynomial of degree l and it is denoted by P_l. For brevity, we will make use of the following notation:

$$\Psi_i^{l,0}(r) = \Psi_i^l(r), \tag{42a}$$

$$\Psi_i^{l,0;\wp} = \Psi_i^{l;\wp}, \tag{42b}$$

where Ψ can be any of the field quantities.

A. Spectral expansion of the elastic displacement field of incident mechanical time harmonic P wave

Recall that the displacement field in the polymer matrix due to the incident P wave is assumed to have the following form:

$$\bar{\mathbf{u}}^{I(2)}(\mathbf{x}, t) = \Lambda e^{\iota(K_p z - \omega t)} \mathbf{e}_z = \Lambda e^{\iota K_p z} e^{-\iota \omega t} \mathbf{e}_z$$

$$= \mathbf{u}^{I(2)}(\mathbf{x}) e^{-\iota \omega t}, \tag{43}$$

where

$$\mathbf{u}^{I(2)}(\mathbf{x}) = \Lambda e^{\iota K_p z} \mathbf{e}_z = \Lambda e^{\iota K_p r \cos \theta} (\mathbf{e}_r \cos \theta - \mathbf{e}_\theta \sin \theta)$$

$$= \Lambda \left[\frac{\partial}{\partial r} (e^{\iota K_p r \cos \theta}) \frac{\mathbf{e}_r}{i K_p} + \frac{\partial}{\partial \theta} (e^{\iota K_p r \cos \theta}) \frac{\mathbf{e}_\theta}{i K_p r} \right]. \tag{44}$$

Now, considering that (see, e.g., Ref. [38])

$$e^{\iota K_p r \cos \theta} = e^{\iota K_p z} = \sum_{l=0}^{\infty} (2l + 1) \iota^l j_l(K_p r) P_l(\cos \theta), \tag{45}$$

where j_l is the spherical Bessel function of order l, we may write

$$\mathbf{u}^{I(2)}(\mathbf{x}) = \Lambda \sum_{l=0}^{\infty} \left[(2l + 1) \iota^l \frac{\partial}{\partial r} (j_l(K_p r)) P_l(\cos \theta) \frac{e_r}{\iota K_p} \right.$$

$$\left. + (2l + 1) \iota^l j_l(K_p r) \frac{\partial}{\partial \theta} (P_l(\cos \theta)) \frac{e_\theta}{\iota K_p r} \right]. \tag{46}$$

This together with the fact that vector spherical harmonics [Eqs. (A2a)–(A2c)] for $m = 0$ take the form

$$\mathbf{V}_1^l(\Omega) = P_l(\cos \theta) \mathbf{e}_r, \tag{47}$$

$$\mathbf{V}_2^l(\Omega) = \frac{\partial}{\partial \theta} (P_l(\cos \theta)) \mathbf{e}_\theta, \tag{48}$$

$$\mathbf{V}_3^l(\Omega) = \frac{\partial}{\partial \theta} (P_l(\cos \theta)) \mathbf{e}_r \times \mathbf{e}_\theta, \tag{49}$$

allow us to write

$$\mathbf{u}^{I(2)}(\mathbf{x}) = \sum_{l=0}^{\infty} [u_1^{l;I(2)}(r) \mathbf{V}_1^l(\Omega) + u_2^{l;I(2)}(r) \mathbf{V}_2^l(\Omega)], \tag{50}$$

where for $l \geqslant 1$

$$u_1^{l;I(2)}(r) = -(2l + 1) \iota^{l+1} \left(j_{l-1}(K_P r) - \frac{l+1}{K_P r} j_l(K_P r) \right), \tag{51}$$

$$u_2^{l;I(2)}(r) = -(2l + 1) \iota^{l+1} \frac{j_l(K_P r)}{K_P r}. \tag{52}$$

In deriving Eq. (51), we used the known recursive relation $\frac{d j_l(z)}{dz} = j_{l-1}(z) - \frac{l+1}{z} j_l(z)$ for $l \geqslant 1$.

B. Spectral strain-displacement relation

Recall from Eq. (39) that $\boldsymbol{\epsilon}(r, \Omega) = \sum_{l=0}^{\infty} \sum_{i=1}^{6} \epsilon_i^l(r) T_i^l(\Omega)$. Using Eq. (7) and the expression for $\nabla_{\mathbb{R}^3}$ in spherical coordinates, the strain-displacement relations in

$\Gamma_1 \cup \Gamma_2$ can be written as

$$\epsilon_1^l(r) = \frac{du_1^l(r)}{dr},$$

$$\epsilon_2^l(r) = \frac{u_1^l(r)}{r} - \frac{1}{2}l(l+1)\frac{u_2^{l,m}(r)}{r},$$

$$\epsilon_3^l(r) = \frac{1}{2}\frac{u_1^l(r)}{r} + \frac{1}{2}r\frac{d}{dr}\left(\frac{u_2^l(r)}{r}\right),$$

$$\epsilon_4^l(r) = \frac{u_2^l(r)}{r},$$

$$\epsilon_5^l(r) = \frac{1}{2}r\frac{d}{dr}\left(\frac{u_3^l(r)}{r}\right),$$

$$\epsilon_6^l(r) = -\frac{u_3^l(r)}{r}. \tag{53}$$

Moreover, Eqs. (28a)–(28e), (40), and (41) can be used to obtain the following strain-displacement relations for the surface/interface:

$$\epsilon_1^{l;\wp}(R) = 0,$$

$$\epsilon_2^{l;\wp}(R) = \frac{u_1^{l;\wp}(R)}{R} - \frac{1}{2}l(l+1)\frac{u_1^{l;\wp}(R)}{R},$$

$$\epsilon_3^{l;\wp}(R) = 0,$$

$$\epsilon_4^{l;\wp}(R) = \frac{u_2^{l;\wp}(R)}{R},$$

$$\epsilon_5^{l;\wp}(R) = 0,$$

$$\epsilon_6^{l;\wp}(R) = -\frac{u_3^{l;\wp}(R)}{R}. \tag{54}$$

Here, $R = R_1$ if $\wp$ represents the free surface and $R = R_2$ if $\wp$ represents the interface.

C. Spectral constitutive relations

It follows directly from Eqs. (15), (37), (38), and (39) that the spectral constitutive relations for the spherically isotropic piezoelectric shell can be written as

$$\sigma_1^l(r) = C_{33}\epsilon_1^l(r) + 2C_{13}\epsilon_2^l(r) - e_{33}E_1^l(r),$$

$$\sigma_2^l(r) = C_{13}\epsilon_1^l(r) + (C_{11} + C_{12})\epsilon_2^l(r) - e_{31}E_1^l(r),$$

$$\sigma_3^l(r) = 2C_{44}\epsilon_3^l(r) - e_{15}(E_2^l(r) + E_3^l(r)),$$

$$\sigma_4^l(r) = (C_{11} - C_{12})\epsilon_4^l(r),$$

$$\sigma_5^l(r) = 2C_{44}\epsilon_5^l(r),$$

$$\sigma_6^l(r) = (C_{11} - C_{12})\epsilon_6^l(r),$$

$$D_1^{l,m}(r) = e_{33}\epsilon_1^{l,m}(r) + 2e_{31}\epsilon_2^l(r) + \kappa_{33}E_1^l(r),$$

$$D_2^l(r) = 2e_{15}\epsilon_3^l(r) + \kappa_{11}E_2^l(r),$$

$$D_3^l(r) = 2e_{15}\epsilon_5^l(r) + \kappa_{11}E_3^l(r),$$

$$B_1^l(r) = \mu_{33}H_1^l(r),$$

$$B_2^l(r) = \mu_{11}H_2^l(r),$$

$$B_3^l(r) = \mu_{11}H_3^l(r). \tag{55}$$

Likewise, using Eqs. (16), (37), (38), and (39), the spectral constitutive relations of the isotropic polymer matrix in the spherical coordinate system are given by

$$\sigma_1^l(r) = (\lambda + 2\mu)\epsilon_1^l(r) + 2\lambda\epsilon_2^l(r),$$

$$\sigma_2^l(r) = \lambda\epsilon_1^l(r) + 2(\lambda + \mu)\epsilon_2^l(r),$$

$$\sigma_3^l(r) = 2\mu\epsilon_3^l(r),$$

$$\sigma_4^l(r) = 2\mu\epsilon_4^l(r),$$

$$\sigma_5^l(r) = 2\mu\epsilon_5^l(r),$$

$$\sigma_6^l(r) = 2\mu\epsilon_6^l(r),$$

$$D_1^l(r) = \kappa_m E_1^l(r),$$

$$D_2^l(r) = \kappa_m E_2^l(r),$$

$$D_3^l(r) = \kappa_m E_3^l(r),$$

$$B_1^l(r) = \mu_m H_1^l(r),$$

$$B_2^l(r) = \mu_m H_2^l(r),$$

$$B_3^l(r) = \mu_m H_3^l(r). \tag{56}$$

Finally, Eqs. (31a)–(31e), (40), and (41) can be used to obtain the spectral constitutive relations of the spherically isotropic surface/interface:

$$\sigma_2^{l;\wp} = (C_{11}^\wp + C_{12}^\wp)\epsilon_2^{l;\wp}, \tag{57}$$

$$\sigma_4^{l;\wp} = (C_{11}^\wp - C_{12}^\wp)\epsilon_4^{l;\wp}, \tag{58}$$

$$\sigma_6^{l;\wp} = (C_{11}^\wp - C_{12}^\wp)\epsilon_6^{l;\wp}, \tag{59}$$

$$P_2^{l;\wp} = \kappa_{11}^\wp E_2^{l;\wp}, \tag{60}$$

$$P_3^{l;\wp} = \kappa_{11}^\wp E_3^{l;\wp}. \tag{61}$$

Recall from Sec. III that $\sigma_1^{l;\wp} = \sigma_3^{l;\wp} = \sigma_5^{l;\wp} = P_1^{l;\wp} = 0$

V. SPECTRAL MEE EQUATIONS

By expanding the MEE fields in terms of the vector and tensor spherical harmonics, the spectral representation of the fully coupled elastodynamics and Maxwell's equations (5), (6a), and (6b) can be written as

$$\frac{d\sigma_1^l(r)}{dr} + 2\frac{\sigma_1^l(r)}{r} - 2\frac{\sigma_2^l(r)}{r} - l(l+1)\frac{\sigma_3^l(r)}{r} = -\rho\omega^2 u_1^l(r), \tag{62}$$

$$\frac{d\sigma_3^l(r)}{dr} + \frac{\sigma_2^l(r)}{r} + 3\frac{\sigma_3^l(r)}{r} - \frac{1}{2}(l-1)(l+2)\frac{\sigma_4^l(r)}{r}$$
$$= -\rho\omega^2 u_2^l(r), \tag{63}$$

$$\frac{d\sigma_5^l(r)}{dr} + 3\frac{\sigma_5^l(r)}{r} + \frac{1}{2}(l-1)(l+2)\frac{\sigma_6^l(r)}{r} + \rho b_3^l(r)$$
$$= -\rho\omega^2 u_3^l(r), \tag{64}$$

$$l(l+1)\frac{H_3^l(r)}{r} = \iota\omega D_1^l(r), \tag{65a}$$

$$\frac{dH_3^l(r)}{dr} + \frac{H_3^l(r)}{r} = \iota\omega D_2^l(r), \tag{65b}$$

$$\frac{H_1^l(r)}{r} - \frac{dH_2^l(r)}{dr} - \frac{H_2^l(r)}{r} = \iota\omega D_3^l(r), \tag{65c}$$

$$l(l+1)\frac{E_3^l(r)}{r} = -\iota\omega B_1^l(r), \tag{65d}$$

$$\frac{dE_3^l(r)}{dr} + \frac{E_3^l(r)}{r} = -\iota\omega B_2^l(r), \tag{65e}$$

$$\frac{dE_2^l(r)}{dr} + \frac{E_2^l(r)}{r} - \frac{E_1^l(r)}{r} = \iota\omega B_3^l(r). \tag{65f}$$

VI. SPECTRAL INTERFACE BOUNDARY CONDITIONS

By expanding the MEE fields appearing in Eqs. (25a)–(25d) in terms of spherical harmonics, the corresponding spectral surface/interface boundary conditions are obtained as follows:

$$[u_1] = [u_2] = [u_3] = 0, \tag{66}$$

$$\left[\sigma_1^l(R)\right] - 2\frac{\sigma_2^{l;\wp}(R)}{R} = -\rho^\wp\omega^2 u_1^l(R), \tag{67}$$

$$\left[\sigma_3^l(R)\right] + \frac{1}{R}\left(\sigma_2^{l;\wp}(R) - \frac{1}{2}(l-1)(l+2)\sigma_4^{l;\wp}(R)\right)$$
$$= -\rho^\wp\omega^2 u_2^l(R), \tag{68}$$

$$\left[\sigma_5^l(R)\right] + \frac{1}{2R}(l-1)(l+2)\sigma_6^{l;\wp}(R) = -\rho^\wp\omega^2 u_3^l(R), \tag{69}$$

$$\left[E_2^l(R)\right] = \left[E_3^l(R)\right] = 0, \tag{70}$$

$$\left[H_2^l(R)\right] + \iota\omega P_3^{l;\wp}(R) = 0, \tag{71}$$

$$\left[H_3^l(R)\right] - \iota\omega P_2^{l;\wp}(R) = 0. \tag{72}$$

VII. SOLUTION OF THE GOVERNING SPECTRAL BVP

In the subsequent sections, we will solve the governing spectral BVP described in Secs. V and VI. In our analysis of the governing spectral BVP, in order to eliminate the possibility of incoming waves which originate at infinity, it is assumed that the components of the electric and magnetic fields satisfy Sommerfeld's radiation condition (see, e.g., Refs. [39,40]).

A. Scattered fields in the polymer matrix region $\Gamma^{(2)}$

A striking result of Theorem 1 proved in Appendix. F, tells us that the solution arising from the differential equations and boundary conditions described in Secs. V and VI together with the constitutive equations given in Sec. IV C, correspond to the harmonics $m = 0$, $l \geqslant 0$. Thus, in general, the solutions can readily be obtained as a superposition of solutions corresponding to each l.

We can use Eqs. (53), (56), (62), and (63) to recover Eq. (11) of Ref. [35] for the scattered mechanical displacement in the polymer matrix:

$$u_1^{l;\Im(2)}(r) = a_l\frac{\partial}{\partial r}[h_l(K_P r)] + b_l l(l+1)\frac{h_l(K_S r)}{r}, \tag{73}$$

$$u_2^{l;\Im(2)}(r) = a_l\frac{h_l(K_P r)}{r} + \frac{b_l}{r}\frac{\partial}{\partial r}[rh_l(K_S r)], \tag{74}$$

where a_l and b_l are constants which will be determined by imposing the boundary conditions. By using Eqs. (56), (65a), (65b), (65f), we arrive at the following equation for the scattered electromagnetic fields:

$$\left(\frac{d^2}{dr^2} + \frac{2}{r}\frac{d}{dr} - \frac{l(l+1)}{r^2} + \mu_m g_m\omega^2\right)H_3^{l;\Im(2)}(r) = 0. \tag{75}$$

In view of the Sommerfeld's radiation condition, the solution of the above equation is

$$H_3^{l;\Im(2)}(r) = \chi_l h_l(K_m r). \tag{76}$$

Subsequently, by using Eqs. (56), (65a), and (65b), we obtain the following relations:

$$E_1^{l;\Im(2)}(r) = -\frac{\iota\chi_l l(l+1)}{r\omega\kappa_m}h_l(K_m r), \qquad l \geqslant 0, \tag{77}$$

$$E_2^{l;\Im(2)}(r) = -\frac{\iota\chi_l}{2\omega\kappa_m}\bigg(K_m(h_{l-1}(K_m r) + h_{l+1}(K_m r))$$
$$+ \frac{h_l(K_m r)}{r}\bigg), \quad l \geqslant 1. \tag{78}$$

B. Refracted fields in the piezoelectric shell region $\Gamma^{(1)}$

1. The mode corresponding to $l = 0$

When $l = 0$, $Y^{0,0}(\Omega) = 1$, and so according to Eqs. (A2a), (A2b), and (A2c), we have

$$\mathbf{V}_1^0(\Omega) = 1\mathbf{e}_r, \quad \mathbf{V}_2^0(\Omega) = 0, \quad \mathbf{V}_3^0(\Omega) = 0. \tag{79}$$

Also, since the curl of any vector field of the form $f(r)\mathbf{e}_r$ is zero, it follows from the spectral strain-displacement relation (53) and Eq. (65a) that

$$\epsilon_1^{0;\Re(2)}(r) = \frac{du_1^{0;\Re(1)}(r)}{dr}, \tag{80}$$

$$\epsilon_2^{0;\Re(2)}(r) = \frac{u_1^{0;\Re(1)}(r)}{r}, \tag{81}$$

$$D_1^{0;\Re(1)}(r) = 0, \tag{82}$$

$$B_1^{0;\Re(1)}(r) = 0. \tag{83}$$

Now, using Eqs. (82) and (83), we obtain

$$E_1^{0;\Re(1)}(r) = -\frac{1}{\kappa_{33}r}\left(2e_{31}u_1^{0;\Re(1)}(r) + e_{33}r\frac{du_1^{0;\Re(1)}(r)}{dr}\right), \tag{84}$$

$$H_1^{0;\Re(1)}(r) = 0. \tag{85}$$

Also, considering Eq. (55) the constitutive equations will take the form

$$\sigma_1^{0;\Re(1)}(r) = C_{33}\epsilon_1^{0;\Re(1)}(r) + 2C_{13}\epsilon_2^{0;\Re(1)}(r) \\ - e_{33}E_1^{0;\Re(1)}(r), \tag{86}$$

$$\sigma_2^{0;\Re(1)}(r) = C_{13}\epsilon_1^{0;\Re(1)}(r) + (C_{11} + C_{12})\epsilon_2^{0;\Re(1)}(r) \\ - e_{31}E_1^{0;\Re(1)}(r). \tag{87}$$

Equations (84)–(87) and the mechanical equilibrium equation (62) lead to following Helmholtz equation:

$$r^2\frac{d^2 u_1^{0;\Re(1)}(r)}{dr^2} + 2r\frac{du_1^{0;\Re(1)}(r)}{dr} - \tilde{\mathcal{A}}u_1^{0;\Re(1)}(r) \\ = -\tilde{\mathcal{B}}^2 r^2 u_1^{0;\Re(1)}(r), \tag{88}$$

in which

$$\tilde{\mathcal{A}} = 2\frac{\kappa_{33}(C_{11} + C_{12} - C_{13}) + e_{31}(2e_{31} - e_{33})}{\kappa_{33}C_{33} + e_{33}^2}, \tag{89a}$$

$$\tilde{\mathcal{B}}^2 = \frac{\rho\omega^2\kappa_{33}}{\kappa_{33}C_{33} + e_{33}^2}. \tag{89b}$$

The solution of equation (88) is

$$u_1(r) = \alpha_5 j_\varsigma(\tilde{\mathcal{B}}r) + \alpha_6 y_\varsigma(\tilde{\mathcal{B}}r), \tag{90}$$

where

$$\varsigma = \frac{\sqrt{1 + 4\tilde{\mathcal{A}}} - 1}{2}. \tag{91}$$

Now, it follows from Eq. (84) that

$$E_1^{0;\Re(1)}(r) = -\frac{\alpha_5}{\kappa_{33}r}\left(2e_{31}j_\varsigma(\tilde{\mathcal{B}}r) + e_{33}r\frac{dj_\varsigma(\tilde{\mathcal{B}}r)}{dr}\right) \\ - \frac{\alpha_6}{\kappa_{33}r}\left(2e_{31}y_\varsigma(\tilde{\mathcal{B}}r) + e_{33}r\frac{dy_\varsigma(\tilde{\mathcal{B}}r)}{dr}\right). \tag{92}$$

2. Modes corresponding to $l \geqslant 1$

Equations (53), (55), (62), (63), (65a), (65b), and (65f) result in the following system of linear ODEs:

$$\mathbf{Q_0}r^2\mathbf{X}'' + \mathbf{Q_1}r\mathbf{X}' + (\mathbf{Q_2} + \mathbf{Q_3}r^2)\mathbf{X} = 0, \tag{93}$$

for the unknown

$$\mathbf{X}(r) = \left\{u_1^{l;\Re(1)}(r), u_2^{l;\Re(1)}(r), H_3^{l;\Re(1)}(r)\right\}^T. \tag{94}$$

Here $\mathbf{Q}_i = q_{ijk}\mathbf{e}_j \otimes \mathbf{e}_k$ where the coefficients q_{ijk} cam be computed in terms of various constants appearing in constitutive relations (see Appendix G). Equation (93) can be readily converted into the following system of first-order equations:

$$r\mathbf{X}' - \mathbf{Z} = 0, \tag{95}$$

$$r^2\mathbf{Z}' + (\mathbf{Q_0}^{-1}\mathbf{Q_1} - \mathbf{I})r\mathbf{Z} + \mathbf{Q_0}^{-1}(\mathbf{Q_2} + \mathbf{Q_3}r^2)\mathbf{X} = 0. \tag{96}$$

The above system can be rewritten as

$$r\{\mathbf{X}', \mathbf{Z}'\}^T = \mathbf{P}\{\mathbf{X}, \mathbf{Z}\}^T, \tag{97}$$

where

$$\mathbf{P} = \begin{bmatrix} 0 & \mathbf{I} \\ -\mathbf{Q_0}^{-1}(\mathbf{Q_2} + \mathbf{Q_3}r^2) & \mathbf{I} - \mathbf{Q_0}^{-1}\mathbf{Q_1} \end{bmatrix}. \tag{98}$$

In order to solve the above system, we write

$$\{\mathbf{X}, \mathbf{Z}\}^T = \sum_{i=0}^{\infty}\mathbf{F}_i r^{\xi+i}, \tag{99}$$

$$\mathbf{F}_i = \{c_{\mathbf{X}_i}, c_{\mathbf{Z}_i}\}^T \qquad \text{For all} \quad i \geqslant 0. \tag{100}$$

Substituting Eq. (99) into the Eq. (97) gives

$$\sum_{i=0}^{\infty}(\xi + i)\mathbf{F}_i r^{\xi+i} = \mathbf{P_0}\sum_{i=0}^{\infty}\mathbf{F}_i r^{\xi+i} + \mathbf{P_1}\sum_{i=0}^{\infty}\mathbf{F}_i r^{\xi+i+2}, \tag{101}$$

where

$$\mathbf{P_0} = \begin{bmatrix} 0 & \mathbf{I} \\ -\mathbf{Q_0}^{-1}\mathbf{Q_2} & \mathbf{I} - \mathbf{Q_0}^{-1}\mathbf{Q_1} \end{bmatrix} \tag{102}$$

and

$$\mathbf{P_1} = \begin{bmatrix} 0 & 0 \\ -\mathbf{Q_0}^{-1}\mathbf{Q_3} & 0 \end{bmatrix}. \tag{103}$$

Consequently,

$$i = 0 \rightarrow \xi\mathbf{F}_0 = \mathbf{P_0}\mathbf{F}_0, \tag{104}$$

$$i = 1 \rightarrow (\xi + 1)\mathbf{F}_1 = \mathbf{P_0}\mathbf{F}_1, \tag{105}$$

$$i \geqslant 2 \rightarrow (\xi + i)\mathbf{F}_i = \mathbf{P_0}\mathbf{F}_i + \mathbf{P_1}\mathbf{F}_{i-2}. \tag{106}$$

It is clear from Eq. (104) that ξ must be an eigenvalue and $\mathbf{F_0}$ must be a corresponding eigenvector of the matrix $\mathbf{P_0}$. In all the applications that we will consider in the present work, the matrix $\mathbf{P_0}$ has 6 distinct eigenvalues whose differences are not integers. In this case, the terms involving odd values of i will disappear. Although, the above formulation is sufficient for the analysis of physical models studied in the present work, it is noteworthy that a rigorous analysis of the case where $\mathbf{P_0}$ does not have 6 distinct eigenvalues or the differences between eigenvalues are integers can be found in books on ordinary differential equations such as Refs. [41,42].

Now, notice that it follows from Eq. (106) that for $i \geqslant 2$

$$\mathbf{F}_i = ((\xi + i)\mathbf{I} - \mathbf{P_0})^{-1}\mathbf{P_1}\mathbf{F}_{i-2}. \tag{107}$$

This recursive formula will give us the general solution to Eq. (97). The arbitrary constants appearing in the solution will be determined by imposing the boundary conditions described in Sec. VI.

C. Refracted fields in region $\Gamma^{(0)}$

We can write the equations for refracted electromagnetic fields in region $\Gamma^{(0)}$ as below:

$$\left(\frac{d^2}{dr^2} + \frac{2}{r}\frac{d}{dr} - \frac{l(l+1)}{r^2} + \mu_0\kappa_0\omega^2\right)H_3^{l;\Re(0)}(r) = 0. \tag{108}$$

The solution of the above equations in $\Gamma^{(0)}$ is

$$H_3^{l;\Re(0)}(r) = \chi_l j_l(K_0 r). \tag{109}$$

Here we used the fact that the solution must be bounded at $r = 0$.

VIII. EM RADIATED POWER

In this section, we will derive a simple expression for the power of the scattered EM waves in the polymer matrix. The total time-averaged EM radiated power crossing a closed surface Σ is given by [43]

$$\langle \mathbf{P} \rangle = \int_\Sigma \frac{1}{2} \text{Re}[\mathbf{E} \times \mathbf{H}^*] \cdot \mathbf{n} \, dA. \tag{110}$$

Now, considering that the spherical Hankel functions satisfy the asymptotic relation

$$h_l(K_m r) \approx (-\iota)^{l+1} \frac{e^{\iota K_m r}}{K_m r} \quad \text{as} \quad r \to \infty, \tag{111}$$

it follows from Eqs. (76)–(78) that as $r \to \infty$,

$$E_2^l(r) \approx \chi_l(-\iota)^{l+1} \frac{e^{\iota K_m r}}{r \omega \kappa_m}, \tag{112}$$

$$H_3^l(r) \approx \chi_l(-\iota)^{l+1} \frac{e^{\iota K_m r}}{K_m r}. \tag{113}$$

According to the results given in Appendix C,

$$\left\| \mathbf{V}_2^{l,0} \right\|^2 = \left\| \mathbf{V}_3^{l,0} \right\|^2 = 4\pi \frac{l(l+1)}{2l+1}. \tag{114}$$

Subsequently, we arrive at the following expression for $\langle \mathbf{P} \rangle$:

$$\langle \mathbf{P} \rangle = \frac{2\pi}{\sqrt{\kappa_m \mu_m} \kappa_m \omega^2} \sum_{l=1}^\infty \frac{l(l+1)}{2l+1} |\chi_l|^2. \tag{115}$$

It is customary to normalize the EM radiated power by $\langle \mathbf{I}_0 \rangle = \frac{1}{2}\sqrt{\rho_m(\lambda + 2\mu)}\pi\omega^2 R^2 |\Lambda|^2$, where $\langle \mathbf{I}_0 \rangle$ is the time-averaged energy flux of the incident P-wave passing through the cross section obtained from projecting the nanospherical particle onto the xy plane (the plane normal to the propagation direction).

IX. RESULTS AND DISCUSSION

In this section, the robustness of the fully dynamic framework developed in previous sections will be shown by analyzing problems that arise in the study of antennas and filters. It is important to note that, since in our work no simplifying electro-quasi-static approximation was made, an accurate prediction of EM wave propagation is possible. Moreover, our formulation is well-suited for the study of problems at nanoscale due to the fact that we extended the Gurtin-Murdoch theory to MEE surfaces/interfaces. Finally, in order to capture the nanoscale nature of the piezoelectric shell in the problems under consideration, we had to work with P waves with frequencies in THz range.

A. Example1: PZT-4 core embedded in epoxy matrix

This example is taken from Ref. [44] to verify the validity of our results in the special case where the inner radius of the piezoelectric shell is 0 (that is, the case where the medium consists of a polymer matrix surrounding a piezoelectric core) and the core is not necessarily nanosize (the characteristic lengths m_1, m_2, m_3, m_4 in our formulation are set to be zero). We will compare the results obtained from

TABLE I. (a) Electromechanical properties of the piezoelectric shell. (b) Electromechanical properties of the epoxy matrix.

Property	PZT-4
C_{11} (GPa)	139
C_{12}	77.8
C_{13}	74.3
C_{33}	115
C_{44}	25.6
e_{31} (C/m^2)	-5.2
e_{33}	15.1
e_{15}	12.7
$k_{11}(10^{-10}$F/m)	64.64
k_{33}	56.22
$\mu_{11}(10^{-6}$N/A$^2)$	5
μ_{33}	10
ρ (Kg/m^3)	7500
Property	Epoxy
λ (GPa)	4.916
μ (GPa)	1.731
$\kappa_m(10^{-10}$F/m)	0.38
$\mu_m(10^{-6}$N/A$^2)$	2.51
ρ (Kg/m^3)	1202

our fully dynamic with results given in Ref. [44]. It is important to note that the formulation presented in Ref. [44] ignores the surface/interface effects and hence can not be applied to nonosize shells. The properties of PZT-4 core and the epoxy matrix are displayed in Table I. The nondimensional frequency is defined by $\beta = \frac{R\omega}{C_s}$ where C_s is the shear velocity in the matrix. In accordance with Ref. [44] in this example, we take $\beta = 1$. the resulting stresses σ_{rr}, and $\sigma_{r\theta}$ on the interface were calculated as function of θ using our analytical framework and are depicted in Fig. 3. As we see, the curves in the diagram perfectly match those given in Fig. 12 of Ref. [44].

B. Example2: PZT-4 shell embedded in epoxy matrix

For further demonstration of the applications of the formulation developed in this paper, in this example we will consider a spherical PZT-4 shell, with outer radius twice the inner radius, embedded in an epoxy matrix. We will assume
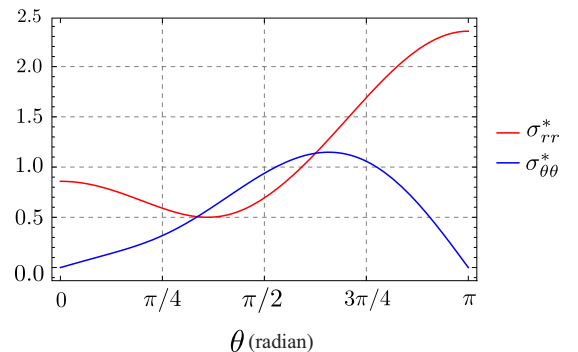

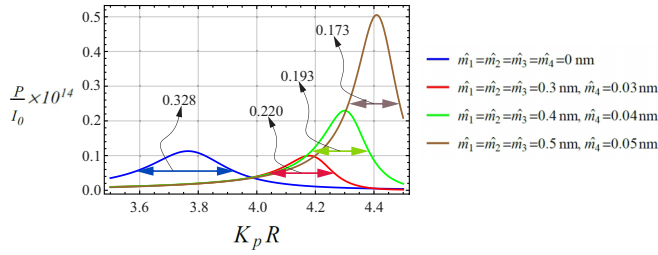FIG. 3. Variations of the nondimensional interface stress in terms of θ.

FIG. 4. Variations in antenna efficiency vs the normalized incident wave number for several choices of characteristic lengths.

FIG. 6. Variations in normalized incident wave number in terms of R for several choices of the characteristic lengths.

the characteristic lengths m_i's, $1 \leqslant i \leqslant 4$ are the same for the free surface and the interface. It is noteworthy that due to the presence of the free surface in addition to the interface, there will be an interference of reflected waves within an ultrathin layer, and the physics of the problem is considerably more complicated compared to the previous example where we only had a solid core. Figure 4 displays the variations in antenna efficiency as the normalized incident wave number ($K_p R$) changes for several choices of characteristic lengths $\hat{m}_1 = \hat{m}_2 = \hat{m}_3$, and $\hat{m}_4$. In this diagram, the outer radius of the shell is taken to be $R = 1$ nm. As it is evident from the diagrams, the frequency corresponding to the fundamental mode resonance increases with the characteristic lengths. Also, the half power bandwidths decrease as the characteristic lengths increase, i.e., 0.328, 0.220, 0.193, and 0.173 in order from right to left. The fact that the antenna efficiency is strongly influenced by the size of the nanoshell is illustrated in Fig. 5. At the nanoscale, the interface and free surface mass densities play a significant role in the antenna efficiency and the frequencies of the fundamental mode resonance. The variations in the antenna efficiency for $\hat{m}_1 = \hat{m}_2 = \hat{m}_3 = 0.5$ nm as $\hat{m}_4$ changes are shown in Fig. 5. Interestingly, as $\hat{m}_4$ becomes larger, the maximum efficiency decreases while the frequency corresponding to the fundamental mode resonance increases. For several classes of characteristic lengths, changes of the normalized incident wave numbers ($K_p R$) corresponding to fundamental mode resonance in terms of R are displayed in Fig. 6. As it can be seen, when the shell size is comparable with the characteristic lengths of the interface, the results are remarkably different from the predictions of the classical theory. Of course, as expected, all the diagrams exhibit the same asymptotic behavior as R increases. The square of the magnitude of the magnetic field representing far-field
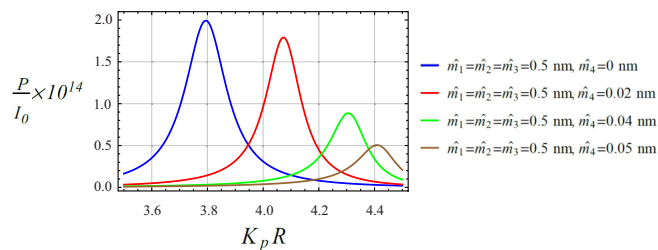
angular pattern radiated from the embedded antenna for different surface and interface properties corresponding to the considered nanosize piezoelectric shell is compared in Fig. 7. As we can see in the plot, various parts of the radiation pattern constitute of what is usually refered to as the major lobes (see, e.g., Ref. [45]). In this figure, power patterns are normalized so that the maximum magnitude of the outermost major lobe is equal to 1. As it is evident from Fig. 7, the major lobes become larger in size as the characteristic lengths increase.

Figures 8–10 display the magnitudes of the magnetic and electric fields, and the magnitudes of the stress components $|\sigma_{r\theta}|$, and $|\sigma_{\theta\theta}|$ throughout the nanovoid, the PZT-4 shell, and the epoxy matrix when the shell is impinged upon by an incident P wave of amplitude $\Lambda = 10^{-3}$ nm. In these figures the characteristic lengths are taken to be $\hat{m}_1 = \hat{m}_2 = \hat{m}_3 = 0.5$ nm, and $\hat{m}_4 = 0.05$ nm. The normalized incident wave number ($K_p R$) used to create these diagrams is 4.4 which corresponds to the wave number associated with the maximum antenna efficiency in the brown curve in Fig. 4. As expected, the magnetic and electric fields in the matrix become weaker as we move away from the center. Moreover, the magnetic field in the PZT-4 shell and the nanovoid has a high value near the free surface at $\theta = \frac{\pi}{2}, \frac{3\pi}{2}$, whereas, the electric field in the PZT-4 shell attains its high values at $\theta = 0, \pi$. The magnitude of the shear stress, $|\sigma_{r\theta}|$, attains its highest value in the proximity of PZT-4 shell/matrix interface at $\theta = \frac{3\pi}{4}, \frac{5\pi}{4}$. Whereas the magnitude of the hoop stress $|\sigma_{\theta\theta}|$ attains its highest value at $\theta = \pi$. The magnitude of the hoop stress, $|\sigma_{\phi\phi}|$, is nearly equal to that of $|\sigma_{\theta\theta}|$, and thus we have refrained from displaying it herein. In Fig. 11, the

FIG. 5. Variations in antenna efficiency versus the normalized incident wave number for several choices of the characteristic length $\hat{m}_4$.
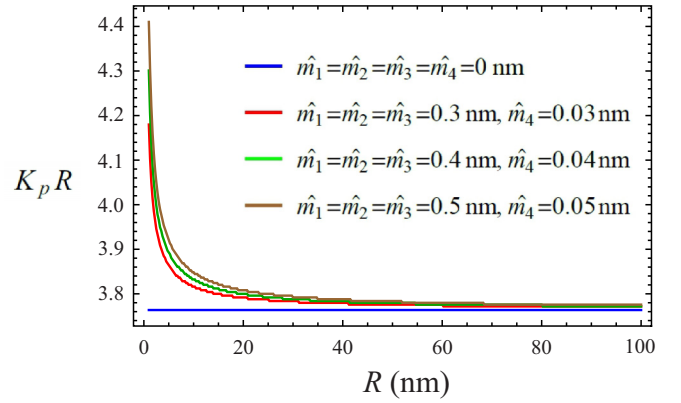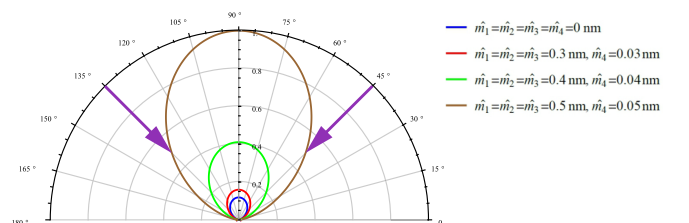

FIG. 7. Far-field angular radiation of the antenna for several choices of the characteristic lengths.
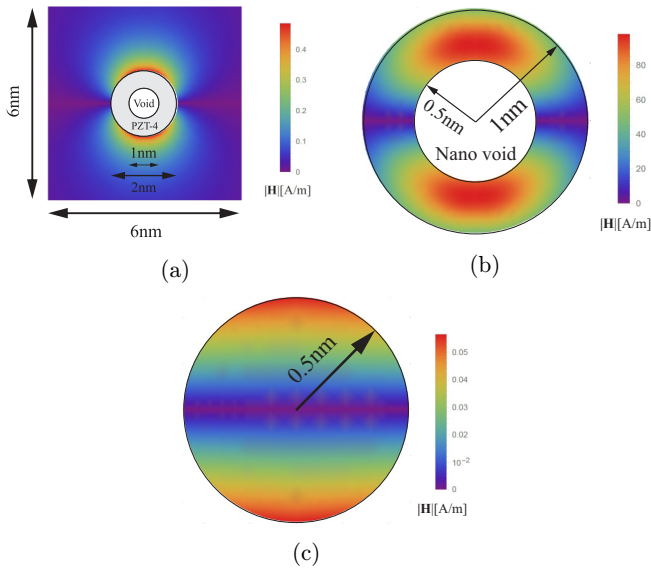
FIG. 8. Distribution of the magnetic field: (a) epoxy matrix, (b) piezoelectric shell, and (c) nanovoid.

normalized angular variations of $\sigma_{\theta\theta}$ and $\sigma_{\phi\phi}$ on the interface and free surface of the considered nano piezoelectric shell are illustrated. The magnitude of polarization on the interface and the free surface against the angular coordinate θ is shown in Fig. 12.
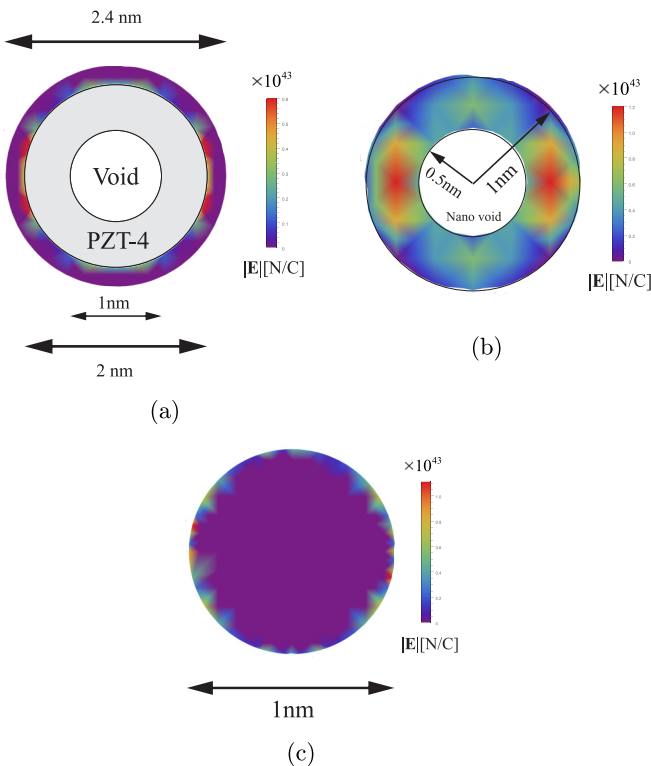

FIG. 9. Distribution of the electric field: (a) epoxy matrix, (b) piezoelectric shell, and (c) nanovoid.
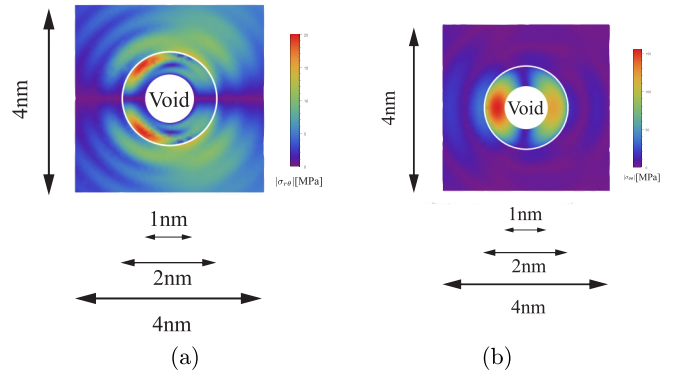

FIG. 10. Distribution of the magnitudes of the stress components: (a) $|\sigma_{r\theta}|$ and (b) $|\sigma_{\theta\theta}|$.

X. CONCLUSION

In conclusion, this study has investigated electromagnetic (EM) radiation emitted from a nanosized spherical piezoelectric scatterer situated in a polymer matrix and exposed to P waves within the THz frequency range. The mathematical analysis and calculations of the scattered MEE fields with high precision were achieved through new formulations of the pertinent electrodynamics equations. More strictly speaking, the bulk of the nanospherical piezoelectric particle and its interface with the surrounding matrix were treated as two separate entities; each entity is mathematically modeled by its own fully coupled elastodynamics and Maxwell's equations. In a way the nanoscopic polarization vector, residual polarization vector, stress field, and the residual stress field appearing on the interface may be considered as the interface conditions. Formulation of the problem of interest within spherical coordinates and utilization of the scalar, vector, and tensor spherical harmonics provided a robust tool for the solution of the fully coupled elastodynamics and Maxwell's equations associated with the interface electrodynamics theory described herein. A noteworthy feature of this theory is its introduction of two distinct characteristic lengths associated with both the elastic and dielectric properties. This allows us to explore the impact of the piezoelectric particle's size on the scattered MEE fields. The size effect was particularly evident in its influence on EM radiated power, the fundamental resonance frequency, and the magnetic field distribution. Our findings underscore that as the size of the piezoelectric fiber approaches the interface characteristic lengths, interface
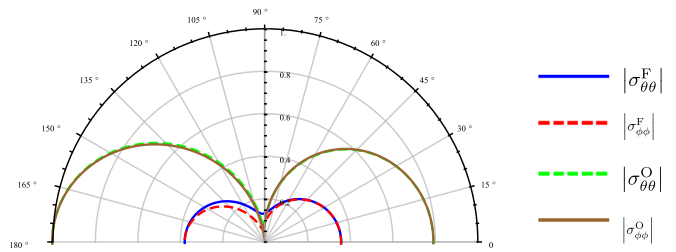

FIG. 11. Normalized angular variations of the inner free surface stresses ($\sigma_{\theta\theta}^{F}$, $\sigma_{\phi\phi}^{F}$) and the outer interface stresses ($\sigma_{\theta\theta}^{O}$, $\sigma_{\phi\phi}^{O}$) in terms of θ.
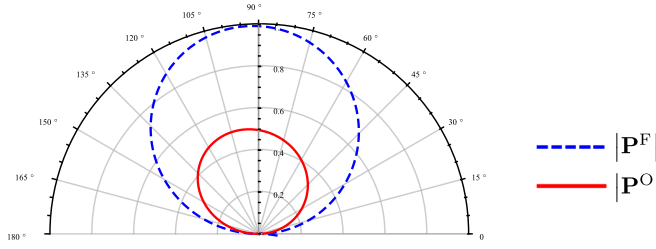
FIG. 12. Variations in the polarization magnitude for, respectively, the inner free surface ($\mathbf{P}^F$) and the outer interface ($\mathbf{P}^O$) in terms of θ.

effects become notably significant. This modeling framework holds promise for the analysis and design of nanosized piezoelectric sensors, resonators, and antennas, making it a valuable tool for future research and applications in this domain.

APPENDIX A: SPHERICAL HARMONICS

Scalar spherical harmonics are functions defined on the surface $\mathbb{S}^2$, the unit sphere in $\mathbb{R}^3$. The collection of scalar spherical harmonics is usually denoted by $\{Y^{l,m}(\Omega)\}_{\substack{l \in \mathbb{N}_0 \\ m \leqslant l}}$. For each $l \in \mathbb{N}_0$ and $|m| \leqslant l$, we have $Y^{l,m}(\Omega) = P_{l,m}(\cos \theta)e^{\iota m \phi}$ where $P_{l,m}(z)$ is the associated Legendre polynomial of degree l and order m. For each $l \in \mathbb{N}_0$ and $|m| \leqslant l$, $Y^{l,m}(\Omega)$ is an eigenfunction of the surface Laplacian on $\mathbb{S}^2$. Indeed,

$$-\nabla_{\mathbb{S}^2}^2 Y^{l,m}(\Omega) = l(l+1)Y^{l,m}(\Omega). \tag{A1}$$

It is noteworthy that the collection of all scalar spherical harmonics $\{Y^{l,m}(\Omega)\}_{\substack{l \in \mathbb{N}_0 \\ m \leqslant l}}$ forms an orthogonal Schauder basis for the space of square-integrable functions on $\mathbb{S}^2$ (see, e.g., Ref. [46], Chap. 7). In Ref. [47], vectorial and tensorial versions of spherical harmonics are introduced, which form a Schauder basis for square-integrable vector fields and second-rank symmetric tensor fields on $\mathbb{S}^2$, respectively. The formulas proposed by Ref. [48], up to some constant normalization factors, are displayed below.

vector spherical harmonics ($l \in \mathbb{N}_0$ and $|m| \leqslant l$):

$$\mathbf{V}_1^{l,m}(\Omega) = Y^{l,m}(\Omega)\mathbf{e}_r, \tag{A2a}$$

$$\mathbf{V}_2^{l,m}(\Omega) = \nabla_{\mathbb{S}^2} Y^{l,m}(\Omega), \tag{A2b}$$

$$\mathbf{V}_3^{l,m}(\Omega) = \mathbf{e}_r \times \nabla_{\mathbb{S}^2} Y^{l,m}(\Omega). \tag{A2c}$$

Note that since $\mathbf{e}_r$ is normal to the sphere and $\mathbf{V}_2^{l,m}(\Omega)$ is tangent to the surface, $\mathbf{V}_3^{l,m}(\Omega) = \mathbf{e}_r \times \nabla_{\mathbb{S}^2} Y^{l,m}(\Omega)$ will be tangent to the sphere.

Second-rank tensor spherical harmonics ($l \in \mathbb{N}_0$ and $|m| \leqslant l$):

$$\mathbf{T}_1^{l,m}(\Omega) = Y^{l,m}(\Omega)\mathbf{e}_r \otimes \mathbf{e}_r, \tag{A3a}$$

$$\mathbf{T}_2^{l,m}(\Omega) = Y^{l,m}(\Omega)\mathbf{e}_\theta \otimes \mathbf{e}_\theta + Y^{l,m}(\Omega)\mathbf{e}_\phi \otimes \mathbf{e}_\phi, \tag{A3b}$$

$$\mathbf{T}_3^{l,m}(\Omega) = 2[\mathbf{e}_r \otimes \nabla_{\mathbb{S}^2} Y^{l,m}(\Omega)]^S, \tag{A3c}$$

$$\mathbf{T}_4^{l,m}(\Omega) = [\nabla_{\mathbb{S}^2} \nabla_{\mathbb{S}^2} Y^{l,m}(\Omega)]^{\text{STT}}, \tag{A3d}$$

$$\mathbf{T}_5^{l,m}(\Omega) = 2[\mathbf{e}_r \otimes (\mathbf{e}_r \times \nabla_{\mathbb{S}^2} Y^{l,m}(\Omega))]^S, \tag{A3e}$$

$$\mathbf{T}_6^{l,m}(\Omega) = -[\mathbf{e}_r \times \nabla_{\mathbb{S}^2} \nabla_{\mathbb{S}^2} Y^{l,m}(\Omega)]^{\text{STT}}. \tag{A3f}$$

In Eqs. (A3a)–(A3f), $[\ldots]^S$ represents the symmetric part of the quantity inside the bracket, and $[\ldots]^{\text{TT}}$ denotes the transverse traceless part of the second order tensor $[\ldots]$ given by

$$[\mathcal{T}_{ab}]^{\text{TT}} = P_{aj}P_{bk}\mathcal{T}_{jk} - \tfrac{1}{2}P_{ab}(P_{jk}\mathcal{T}_{kj}), \tag{A4}$$

in which $P_{jk} = \delta_{jk} - n_j n_k$, where $m, n = 1, 2, 3$, δ_{mn} is the Kronecker delta function, and $\mathbf{n} = \mathbf{e}_r$ is the unit radial vector (see, e.g., Ref. [49]). Some general remarks on eigenfunction expansions in terms of spherical harmonics are discussed in Appendix B. Some useful relations involving spherical harmonics and differential operators such as gradient can be found in Appendix H.

APPENDIX B: EIGENFUNCTION EXPANSIONS

1. Scalar fields

The inner product of two square-integrable scalar fields $f : \mathbb{S}^2 \to \mathbb{R}$ and $g : \mathbb{S}^2 \to \mathbb{R}$ is defined by

$$\langle f, g \rangle = \int_{S^2} f(\Omega)\bar{g}(\Omega)\mathrm{d}\Omega = \int_0^\pi \int_0^{2\pi} f(\Omega)\bar{g}(\Omega)\sin\theta d\phi d\theta. \tag{B1}$$

Here the overbar indicates the complex conjugation. The corresponding norm is given by $\|f\| = \sqrt{\langle f, f \rangle}$. The fact that scalar spherical harmonics are orthogonal with respect to the above inner product tells us that

$$\langle Y^{l_1,m_1}(\Omega), Y^{l_2,m_2}(\Omega) \rangle = \|Y^{l_1,m_1}(\Omega)\| \|Y^{l_2,m_2}(\Omega)\| \delta_{l_1 l_2} \delta_{m_1 m_2},$$

$$l_1, l_2 \geqslant 0, \quad |m_1| \leqslant l_1, \quad |m_2| \leqslant l_2. \tag{B2}$$

An arbitrary square-integrable function f on $\mathbb{S}^2$ can be expressed as

$$f(\Omega) = \sum_{\substack{l \in \mathbb{N}_0 \\ |m| \leqslant l}} \alpha^{l,m} Y^{l,m}(\Omega), \tag{B3}$$

where

$$\alpha^{l,m} = \frac{\langle f, Y^{l,m} \rangle}{\langle Y^{l,m}, Y^{l,m} \rangle}, \tag{B4}$$

and the convergence of the sum is in the mean square sense.

2. Vector fields

Suppose $\mathbf{f}(\Omega)$ is a vector field on $\mathbb{S}^2$. Then, at each point $\Omega \in \mathbb{S}^2$, $\mathbf{f}(\Omega)$ can be represented as

$$\mathbf{f}(\Omega) = f_i(\Omega)\mathbf{e}_i, \tag{B5}$$

where $i = r, \theta, \phi$. The inner product of two square-integrable vector fields $\mathbf{f}(\Omega)$ and $\mathbf{g}(\Omega)$ on $\mathbb{S}^2$ is defined by

$$\langle \mathbf{f}, \mathbf{g} \rangle = \int_{S^2} f_i(\Omega)\bar{g}_i(\Omega)d\Omega. \tag{B6}$$

The corresponding norm is given by $\|\mathbf{f}\| = \sqrt{\langle \mathbf{f}, \mathbf{f} \rangle}$. The fact that vector spherical harmonics are orthogonal with respect to

the above inner product tells us that

$$
\begin{aligned}
&\left\langle V_i^{l_1,m_1}(\Omega), V_j^{l_2,m_2}(\Omega) \right\rangle \\
&= \left\| V_i^{l_1,m_1}(\Omega) \right\| \left\| V_j^{l_2,m_2}(\Omega) \right\| \delta_{ij}\delta_{l_1 l_2}\delta_{m_1 m_2},
\end{aligned}
\tag{B7}
$$

with no summation over the repeated indices. (Here $l_1, l_2 \geqslant 0$, $|m_1| \leqslant l_1$, $|m_2| \leqslant l_2$, $1 \leqslant i, j \leqslant 3$.) An arbitrary square-integrable vector field $\mathbf{f}$ on $\mathbb{S}^2$ can be expressed as

$$
\mathbf{f}(\Omega) = \sum_{\substack{l \in \mathbb{N}_0 \\ |m| \leqslant l}} \sum_{i=1}^{3} \alpha_i^{l,m} V_i^{l,m}(\Omega).
\tag{B8}
$$

where

$$
\alpha_i^{l,m} = \frac{\left\langle \mathbf{f}, V_i^{l,m} \right\rangle}{\left\langle V_i^{l,m}, V_i^{l,m} \right\rangle},
\tag{B9}
$$

and the convergence of the sum is in the mean square sense.

3. Second-order tensor fields

Now, suppose $\mathbf{F}(\Omega)$ is a second-order tensor field on $\mathbb{S}^2$. Then, at each point $\Omega \in \mathbb{S}^2$, $\mathbf{f}(\Omega)$ can be represented as

$$
\mathbf{f}(\Omega) = \mathbf{F}_{i_1 i_2}(\Omega) \mathbf{e}_{i_1} \otimes \mathbf{e}_{i_2},
\tag{B10}
$$

where $i = r, \theta, \phi$. The inner product of two square-integrable vector fields $\mathbf{f}(\Omega)$ and $\mathbf{g}(\Omega)$ on $\mathbb{S}^2$ is defined by

$$
\langle \mathbf{F}, \mathbf{G} \rangle = \int_{S^2} F_{i_1 i_2}(\Omega) \bar{G}_{i_1 i_2}(\Omega) d\Omega,
\tag{B11}
$$

and the corresponding norm is given by $\|\mathbf{F}\| = \sqrt{\langle \mathbf{F}, \mathbf{F} \rangle}$. The fact that tensor spherical harmonics are orthogonal with respect to the above inner product tells us that

$$
\begin{aligned}
&\left\langle T_i^{l_1,m_1}(\Omega), T_j^{l_2,m_2}(\Omega) \right\rangle \\
&= \left\| T_i^{l_1,m_1}(\Omega) \right\| \left\| T_j^{l_2,m_2}(\Omega) \right\| \delta_{ij}\delta_{l_1 l_2}\delta_{m_1 m_2},
\end{aligned}
\tag{B12}
$$

with no summation over the repeated indices. (Here $l_1, l_2 \geqslant 0$, $|m_1| \leqslant l_1$, $|m_2| \leqslant l_2$, $1 \leqslant i, j \leqslant 6$.) An arbitrary square-integrable vector field $\mathbf{F}$ on $\mathbb{S}^2$ can be

expressed as

$$
\mathbf{F}(\Omega) = \sum_{\substack{l \in \mathbb{N}_0 \\ |m| \leqslant l}} \sum_{i=1}^{6} \beta_i^{l,m} T_i^{l,m}(\Omega),
\tag{B13}
$$

where

$$
\alpha_i^{l,m} = \frac{\left\langle \mathbf{F}, T_i^{l,m} \right\rangle}{\left\langle T_i^{l,m}, T_i^{l,m} \right\rangle},
\tag{B14}
$$

and the convergence of the sum is in the mean square sense.

The formulas for the norms of spherical harmonics are given in Appendix C.

APPENDIX C: FORMULAS FOR THE NORMS OF SPHERICAL HARMONICS

Using the formulas given in Appendix B, one can show that [34]

$$
\begin{aligned}
\left\| Y^{l,m}(\Omega) \right\| &= \left\| V_1^{l,m}(\Omega) \right\| = \left\| T_1^{l,m}(\Omega) \right\| \\
&= \frac{1}{\sqrt{2}} \left\| T_2^{l,m}(\Omega) \right\| = \sqrt{\frac{4\pi}{2l+1}\frac{(l+m)!}{(l-m)!}},
\end{aligned}
\tag{C1}
$$

$$
\begin{aligned}
\left\| V_2^{l,m}(\Omega) \right\| &= \left\| V_3^{l,m}(\Omega) \right\| = \frac{1}{\sqrt{2}} \left\| T_3^{l,m}(\Omega) \right\| \\
&= \frac{1}{\sqrt{2}} \left\| T_5^{l,m}(\Omega) \right\| \\
&= \sqrt{l(l+1)\frac{4\pi}{2l+1}\frac{(l+m)!}{(l-m)!}},
\end{aligned}
\tag{C2}
$$

$$
\begin{aligned}
\left\| T_4^{l,m}(\Omega) \right\| &= \left\| T_6^{l,m}(\Omega) \right\| \\
&= \sqrt{\frac{1}{2}(l-1)(l+1)(l+2)\frac{4\pi}{2l+1}}.
\end{aligned}
\tag{C3}
$$

APPENDIX D: A BRIEF OVERVIEW OF STANDARD SURFACE DIFFERENTIAL OPERATORS ON A SPHERE

Consider the case where the surface under consideration, $\wp$, is a sphere of radius R. Let $f : \wp \to \mathbb{R}$ be a smooth scalar field. The surface gradient of f denoted by $\nabla_\wp f$, is given by

$$
\nabla_\wp f = \frac{1}{R}\frac{\partial f}{\partial \theta}\mathbf{e}_\theta + \frac{1}{R\sin\theta}\frac{\partial f}{\partial \phi}\mathbf{e}_\phi.
\tag{D1}
$$

Note that $\nabla_\wp f(\Omega)$ is always a vector field tangent to the sphere. Moreover, the surface gradient of a smooth vector field $\mathbf{v} : \wp \to \mathbb{R}^3$ is given by

$$
\begin{aligned}
\nabla_\wp \mathbf{v}(\Omega) = {}& \frac{1}{R}\left(\frac{\partial v_r(\Omega)}{\partial \theta} - v_\theta(\Omega)\right)\mathbf{e}_\theta \otimes \mathbf{e}_r + \frac{1}{R}\left(v_r(\Omega) + \frac{\partial v_\theta(\Omega)}{\partial \theta}\right)\mathbf{e}_\theta \otimes \mathbf{e}_\theta + \frac{1}{R}\frac{\partial v_\phi(\Omega)}{\partial \theta}\mathbf{e}_\theta \otimes \mathbf{e}_\phi \\
&+ \frac{1}{R}\left(\frac{1}{\sin\theta}\frac{\partial v_r(\Omega)}{\partial \phi} - v_\phi(\Omega)\right)\mathbf{e}_\phi \otimes \mathbf{e}_r + \frac{1}{R}\left(\frac{1}{\sin\theta}\frac{\partial v_\theta(\Omega)}{\partial \phi} - \frac{\cos\theta}{\sin\theta}v_\phi(\Omega)\right)\mathbf{e}_\phi \otimes \mathbf{e}_\theta \\
&+ \frac{1}{R}\left(v_r(\Omega) + \frac{\cos\theta}{\sin\theta}v_\theta(\Omega) + \frac{1}{\sin\theta}\frac{\partial v_\phi(\Omega)}{\partial \phi}\right)\mathbf{e}_\phi \otimes \mathbf{e}_\phi,
\end{aligned}
\tag{D2}
$$

and $\mathcal{D}\mathbf{v}(\Omega)$ [the tangential part of $\nabla_\wp \mathbf{v}(\Omega)$] is given by

$$\mathcal{D}\mathbf{v}(\Omega) = A^{\theta\theta}\mathbf{e}_\theta \otimes \mathbf{e}_\theta + A^{\theta\phi}\mathbf{e}_\theta \otimes \mathbf{e}_\phi + A^{\phi\theta}\mathbf{e}_\phi \otimes \mathbf{e}_\theta + A^{\phi\phi}\mathbf{e}_\phi$$
$$\otimes \mathbf{e}_\phi, \tag{D3}$$

in which

$$A^{\theta\theta} = \frac{1}{R}\left(v_r(\Omega) + \frac{\partial v_\theta(\Omega)}{\partial \theta}\right), \tag{D4}$$

$$A^{\theta\phi} = \frac{1}{R}\frac{\partial v_\phi(\Omega)}{\partial \theta}, \tag{D5}$$

$$A^{\phi\theta} = \frac{1}{R}\left(\frac{1}{\sin\theta}\frac{\partial v_\theta(\Omega)}{\partial \phi} - \frac{\cos\theta}{\sin\theta}v_\phi(\Omega)\right), \tag{D6}$$

$$A^{\phi\phi} = \frac{1}{R}\left(v_r(\Omega) + \frac{\cos\theta}{\sin\theta}v_\theta(\Omega) + \frac{1}{\sin\theta}\frac{\partial v_\phi(\Omega)}{\partial \phi}\right). \tag{D7}$$

The surface divergence of $\mathbf{v} : \wp \to \mathbb{R}^3$ can be computed as follows:

$$\mathrm{div}_\wp \mathbf{v}(\Omega) = \frac{2}{R}v_r(\Omega) + \frac{\cot\theta}{R}v_\theta(\Omega) + \frac{1}{R}\frac{\partial v_\theta(\Omega)}{\partial \theta}$$
$$+ \frac{1}{R\sin\theta}\frac{\partial v_\phi(\Omega)}{\partial \phi}. \tag{D8}$$

Furthermore, divergence of a smooth rank 2 tensor field $\mathbf{T}$ on $\wp$ is given by

$$\mathrm{div}_\wp \mathbf{T} = \frac{1}{R}\left(2T_{rr} - T_{\theta\theta} - T_{\phi\phi} + T_{r\theta}\cot\theta + \csc\theta\frac{\partial T_{r\phi}}{\partial \phi} + \frac{\partial T_{r\theta}}{\partial \theta}\right)\mathbf{e}_r + \frac{1}{R}\left(3T_{r\theta} + (T_{\theta\theta} - T_{\phi\phi})\cot\theta + \csc\theta\frac{\partial T_{\theta\phi}}{\partial \phi} + \frac{\partial T_{\theta\theta}}{\partial \theta}\right)\mathbf{e}_\theta$$
$$+ \frac{1}{R}\left(3T_{r\phi} + 2T_{\theta\phi}\cot\theta + \csc\theta\frac{\partial T_{\phi\phi}}{\partial \phi} + \frac{\partial T_{\theta\phi}}{\partial \theta}\right)\mathbf{e}_\phi. \tag{D9}$$

APPENDIX E: THE WEINGARTEN MAP

Let $\wp$ be an oriented surface whose orientation is specified by the unit normal vector $\mathbf{n}$. The Weingarten map is given by

$$\mathbf{L} = -\nabla_\wp \mathbf{n}. \tag{E1}$$

If the surface $\wp$ is a sphere of radius R oriented with the outward unit normal, then

$$\mathbf{L} = \begin{pmatrix} 0 & 0 & 0 \\ 0 & -\frac{1}{R} & 0 \\ 0 & 0 & -\frac{1}{R} \end{pmatrix}. \tag{E2}$$

APPENDIX F: STIMULATED MODES

In this Appendix, we will prove that u_1^l, u_2^l, and H_3^l are the only nonzero quantities in our spectral MEE equations. In the subsequent subsections, the governing spectral BVP will be solved for these unknowns.

Theorem 1. Consider the BVP described in Secs. V and VI together with the constitutive equations given in Sec. IV C. Assuming that the components of $\mathbf{E}$ satisfy the Sommerfeld's radiation condition, the spectral coefficients $\{u_i^l, E_i^l, D_i^l\}_{\substack{i=3 \\ l\geqslant 0}}$ and $\{H_i^l, B_i^l\}_{\substack{i=1,2 \\ l\geqslant 0}}$ are all equal to zero.

Proof. First, it follows from Eqs. (36), (39), (53), (55), and (64) that $u_3^{l;\Re(1)}$ satisfies the following spherical Bessel differential equation in the region Γ_1:

$$r^2\frac{d^2 u_3^{l;\Re(1)}(r)}{dr^2} + 2r\frac{du_3^{l;\Re}(r)}{dr} - \mathcal{A}u_3^{l;\Re}(r)$$
$$= -\mathcal{B}^2 r^2 u_3^{l;\Re}(r), \tag{F1}$$

where

$$\mathcal{A} = 2 + \frac{1}{2C_{44}}(l+2)(l-1)(C_{11} - C_{12}) \tag{F2}$$

and

$$\mathcal{B}^2 = \frac{\rho\omega^2}{C_{44}}. \tag{F3}$$

The solution to the above equation is

$$u_3^{l;\Re(1)}(r) = \alpha_1 j_{\Theta_1}(\mathcal{B}r) + \alpha_2 y_{\Theta_1}(\mathcal{B}r), \tag{F4}$$

where y_{Θ_1} denotes the spherical Bessel function of the second kind and

$$\Theta_1 = \frac{\sqrt{1+4\mathcal{A}} - 1}{2}. \tag{F5}$$

For the region Γ_2 one can use Eqs. (36), (39), (53), and (56) together with Sommerfeld's radiation condition to recover Eq. (16) of Ref. [44]:

$$u_3^{l;\Im(2)}(r) = c_l h_l(K_S r), \tag{F6}$$

where h_l is the spherical Hankel function of the first kind, and K_S is the shear wave number. Here $C_S = \sqrt{\frac{\mu}{\rho_m}}$.

Since the bounding surface of the nanovoid Γ_0 is traction free, we have $\sigma_5^{l;\Re(0)} = 0$. It follows from the spectral boundary conditions for the nanoshell, given by Eq. (69) at $r = R_2$, Eq. (66), the equality $u_3^{l;I(2)} = 0$, and Eq. (9a) that

$$u_3^{l;\Re(1)}(r) = u_3^{l;\Im(2)}(r) = 0. \tag{F7}$$

Next, by using the Eqs. (37), (38), (55), (65c), (65d), and (65e) in the region Γ_1, we obtain

$$r^2\frac{d^2 E_3^{l;\Re(2)}}{dr^2} + 2r\frac{dE_3^{l;\Re(2)}}{dr} - \hat{\mathcal{A}}E_3^{l;\Re(2)} = -\hat{\mathcal{B}}^2 r^2 E_3^{l;\Re(2)}, \tag{F8}$$

where

$$\hat{\mathcal{A}} = \frac{l(l+1)\mu_{11}}{\mu_{33}} \tag{F9}$$

and

$$\hat{\mathcal{B}}^2 = \kappa_{11}\mu_{11}\omega^2. \tag{F10}$$

The solution to the above equation is

$$E_3^{l;\Re(1)}(r) = \alpha_3 j_{\Theta_2}(\hat{\mathcal{B}}r) + \alpha_4 y_{\Theta_2}(\hat{\mathcal{B}}r), \tag{F11}$$

in which

$$\Theta_2 = \frac{\sqrt{1 + 4\hat{A}} - 1}{2}. \tag{F12}$$

Now, it follows from Eqs. (37), (38), (56), (65c), (65d), and (65e) that $E_3^{l;S(2)}$ satisfies the following spherical Bessel differential equation:

$$\left(\frac{d^2}{dr^2} + \frac{2}{r}\frac{d}{dr} - \frac{l(l+1)}{r^2} + \mu_m g_m \omega^2 \right) E_3^{l;\Im(2)}(r) = 0. \tag{F13}$$

Considering Sommerfeld's radiation condition, the solution of the above equation is

$$E_3^{l;\Im(2)}(r) = a h_l(K_m r), \tag{F14}$$

where $K_m = \frac{\omega}{C_m}$ is the electromagnetic wave number of the matrix, and $C_m = \frac{1}{\sqrt{\mu_m g_m}}$ is speed of the light in the matrix. Furthermore, by the constitutive relations, $D = \kappa_0 E$, and $B = \mu_0 H$, Eqs. (65c), (65d), and (65e) we obtain

$$\left(\frac{d^2}{dr^2} + \frac{2}{r}\frac{d}{dr} - \frac{l(l+1)}{r^2} + \mu_0 \kappa_0 \omega^2 \right) E_3^{l;\Re(0)}(r) = 0. \tag{F15}$$

Since, $E_3^{l;\Re(0)}$ remains bounded as $r \to 0$, the solution of the above equation is

$$E_3^{l;\Re(0)}(r) = b j_l(K_0 r), \tag{F16}$$

where $K_0 = \frac{\omega}{C_0}$ is the electromagnetic wave number of the vacuum and $C_0 = \frac{1}{\sqrt{\mu_0 \kappa_0}}$ is speed of the light in vacuum. Now, by using the spectral surface/interface constitutive equation Eq. (60) and interface condition Eq. (70) for mechanical incident waves we have

$$E_3^{l;\Re(0)}(r) = E_3^{l;\Re(1)}(r) = E_3^{l;\Im(2)}(r) = 0. \tag{F17}$$

Finally, using Eqs. (65d), (65e), we have

$$H_1^{l;\Re(0)}(r) = H_1^{l;\Re(1)}(r) = H_1^{l;\Im(2)}(r) = 0, \tag{F18a}$$

$$H_2^{l;\Re(0)}(r) = H_2^{l;\Re(1)}(r) = H_2^{l;\Im(2)}(r) = 0. \tag{F18b}$$

APPENDIX G: COMPONENTS OF THE TENSORS Q_i

Here, we present explicit expressions for the components of the tensors Q_i ($i = 0, 1, 2, 3$) appearing in Eq. (93)

$$\mathbf{Q}_i = q_{ijk}\mathbf{e}_j \otimes \mathbf{e}_k, \tag{G1}$$

in which $j, k = 1, 2, 3$. We have

$$q_{011} = C_{33} + \frac{e_{33}^2}{\kappa_{33}}, \quad q_{012} = q_{013} = q_{021} = q_{031} = 0,$$

$$q_{022} = q_{44} + \frac{e_{15}^2}{\kappa_{11}}, \quad q_{023} = \frac{\iota e_{15}}{\omega \kappa_{11}}, \quad q_{032} = -\frac{e_{15}}{\kappa_{11}},$$

$$q_{033} = -\frac{\iota}{\omega \kappa_{11}}, \quad q_{111} = 2\left(C_{33} + \frac{e_{33}^2}{\kappa_{33}} \right),$$

$$q_{112} = -l(l+1)\left(C_{13} + C_{44} + \frac{e_{15}^2}{\kappa_{11}} + \frac{e_{31}e_{33}}{\kappa_{33}} \right),$$

$$q_{113} = \frac{l(l+1)\iota}{\omega}\left(\frac{e_{33}}{\kappa_{33}} - \frac{e_{15}}{\kappa_{11}} \right),$$

$$q_{121} = C_{13} + C_{44} + \frac{e_{15}^2}{\kappa_{11}} + \frac{e_{31}e_{33}}{\kappa_{33}},$$

$$q_{122} = 2\left(C_{44} + \frac{e_{15}^2}{\kappa_{11}} \right), \quad q_{123} = 4\frac{\iota e_{15}}{\omega \kappa_{11}},$$

$$q_{131} = \frac{e_{33}}{\kappa_{33}} - \frac{e_{15}}{\kappa_{11}}, \quad q_{132} = 0, \quad q_{133} = -2\frac{\iota}{\omega \kappa_{11}},$$

$$q_{211} = 2C_{13} - l(l+1)\left(\frac{e_{15}^2}{\kappa_{11}} + C_{44} \right)$$
$$- \frac{\left(4e_{31}^2 - 2e_{31}e_{33} + 2(C_{11} + C_{12}) \right)}{\kappa_{33}},$$

$$q_{212} = C_{11} + C_{12} + C_{44} - C_{13} + \frac{2e_{31}^2 - e_{31}e_{33}}{\kappa_{33}} + \frac{e_{15}^2}{\kappa_{11}},$$

$$q_{213} = -\frac{l(l+1)\iota}{\omega}\left(\frac{e_{15}}{\kappa_{11}} + \frac{2e_{31} - e_{33}}{\kappa_{33}} \right),$$

$$q_{221} = C_{11} + C_{12} + 2\frac{e_{31}^2}{\kappa_{33}} + 2\frac{e_{15}^2}{\kappa_{11}},$$

$$q_{222} = -(l^2 + l - 1)C_{11} - C_{12} - 2C_{44}$$
$$- l(l+1)\frac{e_{31}^2}{\kappa_{33}} - 2\frac{e_{15}^2}{\kappa_{11}},$$

$$q_{223} = \frac{\iota}{\omega}\left(l(l+1)\frac{e_{31}}{\kappa_{33}} + 2\frac{e_{15}}{\kappa_{11}} \right), \quad Q_{231} = 2\frac{e_{31}}{\kappa_{33}},$$

$$q_{232} = -l(l+1)\left(\frac{e_{31}}{\kappa_{33}} \right), \quad Q_{233} = \frac{l(l+1)\iota}{\omega \kappa_{33}},$$

$$q_{311} = \rho\omega^2, \quad q_{312} = q_{313} = q_{321} = q_{323} = 0,$$

$$q_{322} = \rho\omega^2, \quad q_{331} = q_{332} = 0, \quad q_{333} = -\iota\omega\mu_{11}.$$

APPENDIX H: SOME RECURSION RELATIONS INVOLVING THE SPHERICAL HARMONICS AND THE OPERATORS CURL AND GRADIENT

$$\text{curl}_{\mathbb{R}^3}(f(r)\mathbf{V}_1^{l,m}(\Omega)) = -\frac{f(r)}{r}\mathbf{V}_3^{l,m}(\Omega), \tag{H1}$$

$$\text{curl}_{\mathbb{R}^3}\big(f(r)\mathbf{V}_2^{l,m}(\Omega)\big) = \left(\frac{df(r)}{dr} + \frac{f(r)}{r}\right)\mathbf{V}_3^{l,m}(\Omega), \tag{H2}$$

$$\text{curl}_{\mathbb{R}^3}\big(f(r)\mathbf{V}_3^{l,m}(\Omega)\big) = -l(l+1)\frac{f(r)}{r}\mathbf{V}_1^{l,m}(\Omega) - \left(\frac{df(r)}{dr} + \frac{f(r)}{r}\right)\mathbf{V}_2^{l,m}(\Omega), \tag{H3}$$

$$\left[\nabla_{\mathbb{R}^3}(f(r)\mathbf{V}_1^{l,m}(\Omega))\right]^S = \frac{df(r)}{dr}\mathbf{T}_1^{l,m}(\Omega) + \frac{f(r)}{r}\mathbf{T}_2^{l,m}(\Omega) + \frac{f(r)}{2r}\mathbf{T}_3^{l,m}(\Omega), \tag{H4}$$

$$\left[\nabla_{\mathbb{R}^3}(f(r)\mathbf{V}_2^{l,m}(\Omega))\right]^S = -\frac{1}{2}l(l+1)\frac{f(r)}{r}\mathbf{T}_2^{l,m}(\Omega) - \frac{1}{2}\left(\frac{f(r)}{r} - \frac{df(r)}{dr}\right)\mathbf{T}_3^{l,m}(\Omega) + \frac{f(r)}{r}\mathbf{T}_4^{l,m}(\Omega), \tag{H5}$$

$$\left[\nabla_{\mathbb{R}^3}(f(r)\mathbf{V}_3^{l,m}(\Omega))\right]^S = \frac{1}{2}\left(\frac{df(r)}{dr} - \frac{f(r)}{r}\right)\mathbf{T}_5^{l,m}(\Omega) - \frac{f(r)}{r}\mathbf{T}_6^{l,m}(\Omega). \tag{H6}$$

[1] M. Zaeimbashi, M. Nasrollahpour, A. Khalifa, A. Romano, X. Liang, H. Chen, N. Sun, A. Matyushov, H. Lin, C. Dong *et al.*, Ultra-compact dual-band smart nems magneto-electric antennas for simultaneous wireless energy harvesting and magnetic field sensing, Nat. Commun. **12**, 3141 (2021).

[2] B. Kramer, C.-C. Chen, M. Lee, and J. Volakis, Fundamental limits and design guidelines for miniaturizing ultra-wideband antennas, IEEE Antennas Propag. Mag. **51**, 57 (2009).

[3] J. Gianvittorio and Y. Rahmat-Samii, Fractal antennas: A novel antenna miniaturization technique, and applications, IEEE Antennas Propag. Mag. **44**, 20 (2002).

[4] P. Ikonen, K. Rozanov, A. Osipov, P. Alitalo, and S. Tretyakov, Magnetodielectric substrates in antenna miniaturization: Potential and limitations, IEEE Trans. Antennas Propag. **54**, 3391 (2006).

[5] H. Mosallaei and K. Sarabandi, Magneto-dielectrics in electromagnetics: Concept and applications, IEEE Trans. Antennas Propag. **52**, 1558 (2004).

[6] M. El Ghzaoui, S. Das, T. R. Lenka, and A. Biswas, *Terahertz Wireless Communication Components and System Technologies* (Springer, Singapore, 2022).

[7] J. Domann and G. Carman, Strain powered antennas, J. Appl. Phys. **121**, 044905 (2017).

[8] R. Mindlin, Electromagnetic radiation from a vibrating quartz plate, Int. J. Solids Struct. **9**, 697 (1973).

[9] P. C. Y. Lee, Electromagnetic radiation from an AT-cut quartz plate under lateral-field excitation, J. Appl. Phys. **65**, 1395 (1989).

[10] A. Ballato, Modeling piezoelectric and piezomagnetic devices and structures via equivalent networks, IEEE Trans. Ultrason. Ferroelectr. Freq. Control **48**, 1189 (2001).

[11] X. Wang, C. J. Summers, and Z. L. Wang, Large-scale hexagonal-patterned growth of aligned zno nanorods for nano-optoelectronics and nanosensor arrays, Nano Lett. **4**, 423 (2004).

[12] L. Zhao, M. Steinhart, M. Yosef, S. K. Lee, and S. Schlecht, Large-scale template-assisted growth of LiNbO$_3$ one-dimensional nanostructures for nano-sensors, Sens. Actuators, B **109**, 86 (2005).

[13] J. H. He, J. H. Hsu, C. W. Wang, H. N. Lin, L. J. Chen, and Z. L. Wang, Pattern and feature designed growth of zno nanowire arrays for vertical devices, J. Phys. Chem. B **110**, 50 (2006).

[14] M. Bibes and A. Barthelemy, Towards a magnetoelectric memory, Nat. Mater. **7**, 425 (2008).

[15] E. Lage, C. Kirchhof, V. Hrkac, L. Kienle, R. Jahns, R. Knoechel, E. Quandt, and D. Meyners, Exchange biasing of magnetoelectric composites, Nat. Mater. **11**, 523 (2012).

[16] G. Srinivasan and Y. Fetisov, Ferrite-piezoelectric layered structures: Microwave magnetoelectric effects and electric field tunable devices, Ferroelectrics **342**, 65 (2006).

[17] Y. Fetisov and G. Srinivasan, Electric field tuning characteristics of a ferrite-piezoelectric microwave resonator, Appl. Phys. Lett. **88**, 143503 (2006).

[18] T. Nan, H. Lin, Y. Gao, A. Matyushov, G. Yu, H. Chen, N. Sun, S. Wei, Z. Wang, M. Li *et al.*, Acoustically actuated ultra-compact nems magnetoelectric antennas, Nat. Commun. **8**, 296 (2017).

[19] M. Gurtin and A. Murdoch, A continuum theory of elastic material surfaces, Arch. Ration. Mech. Anal. **57**, 291 (1975).

[20] M. E. Gurtin, J. Weissmüller, and F. Larché, A general theory of curved deformable interfaces in solids at equilibrium, Philos. Mag. A **78**, 1093 (1998).

[21] X. Fang and J. Liu, Dynamic stress and electric displacement around a nano-fiber in piezoelectric nanocomposites under electro-elastic waves, Philos. Mag. Lett. **91**, 621 (2011).

[22] L. L. Zhang, J. X. Liu, X. Q. Fang, and G. Q. Nie, Surface effects on the scattering of compressional waves by a piezoelectric nano-cylinder, J. Appl. Phys. **115**, 244305 (2014).

[23] L. L. Zhang, J. Zhao, X. L. Liu, and J. X. Liu, Shear horizontal surface waves in piezoelectric materials with surface stress, Philos. Mag. Lett. **98**, 350 (2018).

[24] M. T. Jam and H. M. Shodja, Interface effects on the electromagnetic radiation emanating from an embedded piezoelectric nano-fiber incident upon by sh-waves, Wave Motion **94**, 102513 (2020).

[25] C. Tai, I. Antennas, P. Society, I. M. Theory, and T. Society, *Dyadic Green Functions in Electromagnetic Theory*, IEEE Press Publication Series (IEEE Press, 1994).

[26] Y. Zhou, K. M. Rabe, and D. Vanderbilt, Surface polarization and edge charges, Phys. Rev. B **92**, 041102(R) (2015).

[27] R. E. Camley, Z. Celinski, and R. Stamps, *Magnetism of Surfaces, Interfaces, and Nanoscale Materials* (Elsevier Science, 2016).

[28] A. Freeman, H. Krakauer, S. Ohnishi, D.-S. Wang, M. Weinert, and E. Wimmer, Magnetism at surfaces and interfaces, J. Magn. Magn. Mater. **38**, 269 (1983).

[29] J. S. Townsend, *A Modern Approach to Quantum Mechanics*, International Series in Pure and Applied Physics (University Science Books, 2000).

[30] H. Shodja and A. Khorshidi, Tensor spherical harmonics theories on the exact nature of the elastic fields of a spherically anisotropic multi-inhomogeneous inclusion, J. Mech. Phys. Solids **61**, 1124 (2013).

[31] H. Shodja and A. Khorshidi, Comment on "annular inhomogeneities with eigenstrain and interphase modeling" [2014, J. Mech. Phys. Solids 64, 468–482], J. Mech. Phys. Solids **73**, 1 (2014).

[32] H. M. Shodja, M. Farsiani, and A. Behzadan, Tensor spherical harmonics analysis of electro-elastostatic fields in a spherically isotropic multiphase functionally graded piezoelectric medium, Proc. R. Soc. A **479**, 20230267 (2023).

[33] M. R. S. Z. I. M. Gel'fand, *Representations of the Rotation and Lorentz Groups and Their Applications* (Pergamon Press, Oxford, 1963).

[34] A. Khorshidi and H. Shodja, A spectral theory formulation for elastostatics by means of tensor spherical harmonics, J. Elast. **111**, 67 (2013).

[35] M. Kamali and H. Shodja, The scattering of *p*-waves by a piezoelectric particle with fgpm interfacial layers in a polymer matrix, Int. J. Solids Struct. **47**, 2390 (2010).

[36] C. A. Balanis, *Advanced Engineering Electromagnetics*, CourseSmart Series (Wiley, New York, 2012).

[37] S. Dai, M. Gharbi, P. Sharma, and H. S. Park, Surface piezoelectricity: Size effects in nanostructures and the emergence of piezoelectricity in non-piezoelectric materials, J. Appl. Phys. **110**, 104305 (2011).

[38] K. Cahill, *Physical Mathematics* (Cambridge University Press, Cambridge, 2019).

[39] S. H. Schot, Eighty years of sommerfeld's radiation condition, Hist. Math. **19**, 385 (1992).

[40] C. H. Papas, An application of sommerfeld's complex order wave functions to antenna theory, J. Math. Phys. **33**, 269 (1954).

[41] G. Teschl, *Ordinary Differential Equations and Dynamical Systems*, Graduate Studies in Mathematics (American Mathematical Society, 2012).

[42] A. Coddington and N. Levinson, *Theory of Ordinary Differential Equations*, International Series in Pure and Applied Mathematics (McGraw-Hill, 1955).

[43] J. D. Jackson, *Classical Electrodynamics* (Wiley, New York, 1962).

[44] M. Kamali and H. Shodja, The scattering of electro-elastic waves by a spherical piezoelectric particle in a polymer matrix, Int. J. Eng. Sci. **44**, 633 (2006).

[45] C. A. Balanis, *Antenna Theory: Analysis and Design* (Wiley, New York, 2016).

[46] S. F. Singer, *Linearity, Symmetry, and Prediction in the Hydrogen Atom*, Undergraduate Texts in Mathematics (Springer, New York, 2005).

[47] J. Mathews, Gravitational multipole radiation, J. Soc. Ind. Appl. Math. **10**, 768 (1962).

[48] F. J. Zerilli, Tensor harmonics in canonical form for gravitational radiation and other applications, J. Math. Phys. **11**, 2203 (1970).

[49] K. S. Thorne, Multipole expansions of gravitational radiation, Rev. Mod. Phys. **52**, 299 (1980).